Graphical Abstract

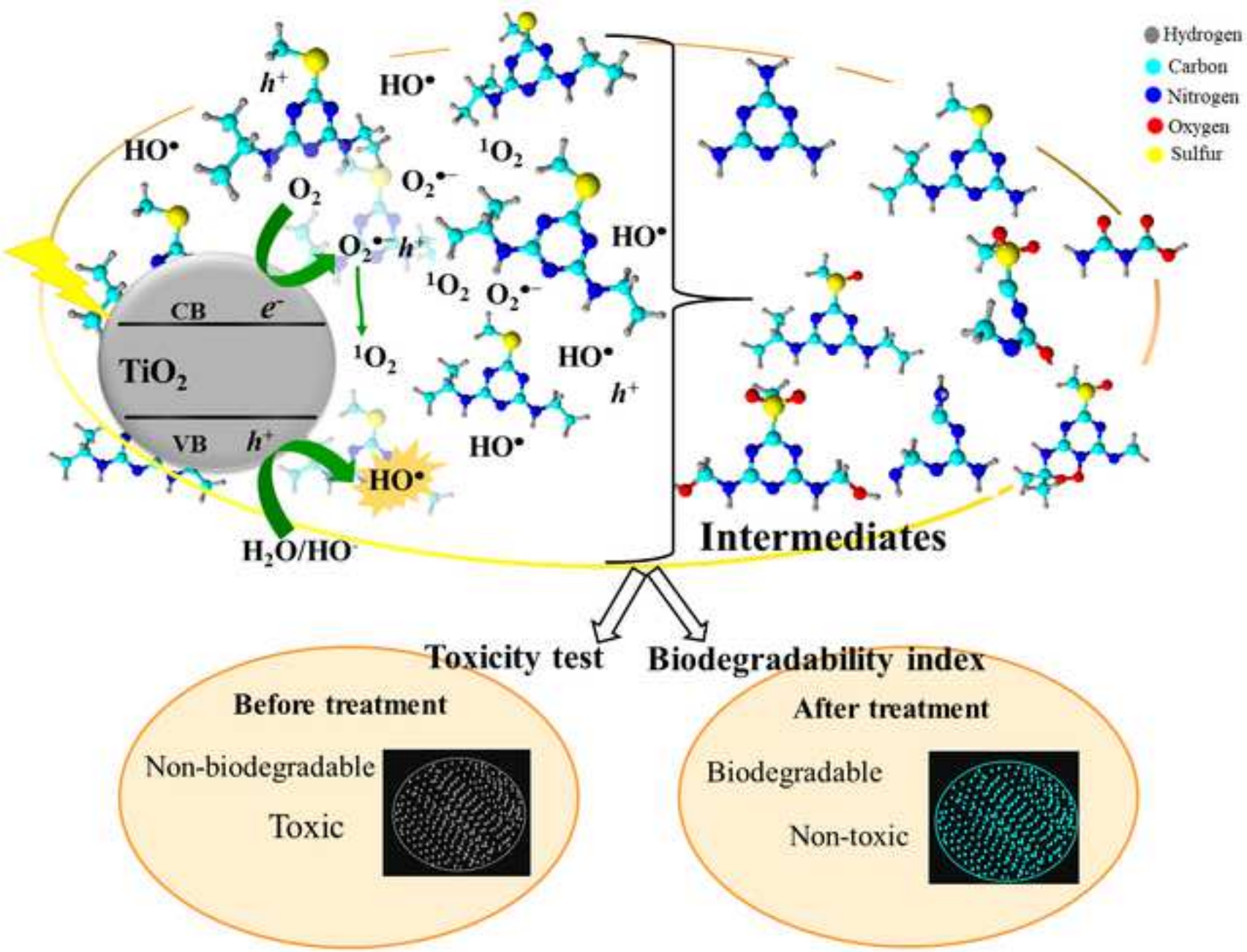

Highlights

- After treatment ametryn solution becomes biodegradable and non-toxic.
- Scavengers were used to elucidate the role of different active species.
- Photocatalytic degradation of ametryn is conducted mainly by $HO^{\bullet}$ radicals.
- Intermediates are differentiated depending on the active species involved.
- Reaction pathways of the ametryn degradation with contributed ROS were proposed.

Evaluation of the main active species involved in the TiO_2 photocatalytic degradation of ametryn herbicide and its by-products

Rodrigo Pereira Cavalcante[1,2], Dirce Martins de Oliveira[3], Lucas de Melo da Silva[1], Jaime Giménez[4], Santiago Esplugas[4], Silvio César de Oliveira[1], Renato Falcao Dantas[2], Carme Sans[4]*, Amilcar Machulek Junior[1,3]**

(1) Institute of Chemistry, Federal University of Mato Grosso do Sul, Av. Senador Filinto Muller, 1555, CP 549, CEP 79074-460- Campo Grande, MS, Brazil.

(2) School of Technology, University of Campinas – UNICAMP, Paschoal Marmo, 1888; CEP 13484-332 – Limeira, SP, Brazil

(3) Faculty of Engineering, Architecture and Urbanism and Geography, Federal University of Mato Grosso do Sul, Cidade Universitária, CP 549, CEP 79070-900 Campo Grande, MS, Brazil.

(4) Department of Chemical Engineering and Analytical Chemistry, Faculty of Chemistry, Universitat de Barcelona, C/Martí i Franqués 1, 08028 Barcelona, Spain

**Corresponding author: E-mail address: machulekjr@gmail.com (A. Machulek Jr.)

*Corresponding author: E-mail address: carmesans@ub.edu (Carme Sans)

Abstract

In this study, we investigated the effectiveness of photocatalysis using TiO_2 as catalyst on the removal of ametryn. The evaluation of photocatalytic activity under simulated sunlight was discussed as evidence by numerous controlled trials and several operational parameters such as ametryn concentration, total organic carbon, chemical oxygen demand, specific UV absorbance, biochemical oxygen demand, toxicity and formed intermediates. Moreover, the roles of reactive species involved in the degradation of ametryn were examined by using different specific scavengers. Ametryn removed by photocatalysis using 0.4 g L^{-1} of TiO_2 was 100% within 60 min, while only 30% was achieved by photolysis at the same time. Biodegradability index improved from 0.3 (raw solution) up to 0.8 while the acute toxicity measured by the inhibition percentage of bioluminescence from *Vibro fischeri* indicates that the photocatalytic treatment promotes 97% of toxicity reduction. The scavenger study shows different percentages of inhibition in ametryn degradation, which allowed to conclude that $HO^{\bullet}$, valence-band holes and $O_2^{\bullet-}$ could intervene in the degradation of ametryn, with predominance of $HO^{\bullet}$. Thirty-eight intermediates were identified from the photocatalytic degradation of ametryn. The comparison of the generation of those intermediates with and without the addition of scavengers showed that different by-products are generated depending on the predominance of the active species. For example, the presence of azide resulted in intermediates formed by condensation reactions. Based on the identified intermediates, reaction pathways and a degradation mechanism were proposed, including $HO^{\bullet}$ radicals, $O_2^{\bullet-}$, holes, and $^1O_2$.

Keywords: Biodegradability; Acute toxicity; kinetics; Scavengers; Reaction mechanism.

1. Introduction

Pesticides are commonly known to be part of the main groups of toxic substances. Thereby, the extensive and inappropriate use of pesticides mainly in agricultural practices results in several negative factors, ranging from contamination of environmental compartments, especially surface- and ground-water bodies and soil, to damage to human health [1,2]. Thus, these compounds are considered emerging contaminants by the scientific communities [3].

These types of compounds are frequently found in the environment, especially in water compartments, in concentrations that range from ng L^{-1} to µg L^{-1} [4]. Although their concentration is low, the consequences of their exposition are unknown in the long term and they are pseudo-persistent in the environment due to their continuous discharge. However, pesticide concentrations in the environment might be exceedingly high, for example, it can reach levels up to 500 mg L^{-1} in wastewaters [5].

Due to their high efficiency in the control of broadleaf and grass weeds, herbicides of the class of triazines are widely used all over the world [6]. They are present in the 10 most widely used pesticides formulations in Europe [7]. As triazines are very stable compounds, they accumulate in environmental compartments for a long time. Another important factor is that triazines are susceptible to leaching from the soils to waterbodies and appear in drinking water. This is favored by their physicochemical properties, including: (i) relatively high water solubility (185 mg L^{-1}, 20 ºC [8]); (ii) low sorption coefficient (316 ~ 445 cm^3 g^{-1} [9]); (iii) high polarity (log K_{ow} 2.7-3.1 [8]); or (iv) long half-life time (70–250 days, varying with type of soil and weather conditions [10]). In addition, these compounds can undergo slow degradation to water-soluble by-products [11]. Among triazines, especial emphasis can be made on ametryn ($C_9H_{17}N_5S$, 2-ethylamino-4-isopropylamino-6-methylthio-s-triazine).

Ametryn is known as an endocrine disrupting compound, which can cause cancerous tumors after long exposition [12]. In addition, other symptoms (nausea, vomiting, diarrhea,

salivation, muscle weakness, irritation to the skin, eyes, and respiratory tract) appear as clinical pictures of ametryn poisoning [12,13]. Triazines are also compounds known to induce oxidative stress, cellular and DNA damage, and cell death [14]. These factors point out that this herbicide represents a risk to the environment and the human health.

Residues of ametryn are sources of contamination of water and soils. Ametryn was detected at 1.56 ± 0.04 μg L^{-1} in groundwater samples in the city of Assis, located in the State of São Paulo (Brazil) [15]. 3.4 mg L^{-1} of ametryn also found in the agricultural runoff water in Veerapur village, Karnataka state, India [16]. In addition, several studies have shown ametryn residues in water and sewage samples at concentrations from ng L^{-1} to μg L^{-1} [17-19]. These examples demonstrate that ametryn residues are introduced into several environmental compartments around the world. Once ametryn is present in water compartments, it would be extremely difficult to be treated. A potential strategy to eliminate emerging contaminants from aqueous solutions involves advanced oxidation processes (AOPs) [20,21]. Among AOPs, heterogeneous photocatalysis can be considered an interesting option due to the low cost and effectiveness to remove micropollutants from water [22-24].

The heterogeneous photocatalysis is defined as a photochemical process in which the semiconducting species is irradiated with light of suitable wavelength (sufficient energy to overcome the band gap) for the promotion of electrons form the valence to the conduction band. Consequently, the reduction and oxidation sites generated can produce different active species, such as hydroxyl ($HO^{\bullet}$), superoxide ($O_2^{\bullet -}$) and perhydroxyl ($HO_2^{\bullet}$) radicals, singlet oxygen ($^1O_2$), H_2O_2, and holes (h_{BV}^+) [25-27], which are the main oxidants responsible for the decomposition reactions of organic compounds.

Among a wide spectrum of semiconductors, TiO_2 is an attractive approach to water purification, mainly due to its excellent performance as photocatalyst, low cost, possibility of activation by sunlight, low toxicity, and long-term stability of the material [28,29]. The most

common commercial TiO_2 is Evonik AEROXIDE® TiO_2 P-25 (denoted as P25). This oxide is comprised of individual anatase and rutile nanoparticles, together with around 15% of rutile formed heterojunction structure with anatase phase [30]. Its main advantage is the numerous oxygen vacancies, which assists the absorption of solar/visible light and the separation of e^-/h^+ pairs [31]. Thus, an increase in the active species implies cost reduction, as it is not necessary to use UV radiation. In this context, photocatalytic treatments using sunlight or UVA, highlighting xenon lamps here, are of great interest for economic reasons.

Although photocatalytic processes are well described in the literature, the contribution of the role of reactive oxygen species (ROS) and holes is debatable and depends on some factors such as, nature of the photocatalyst, source of irradiation, organic contaminant treated, sample constituents and matrices [32,33]. In the literature it is possible to find several works focused on understanding the roles of ROS in the entire degradation system using selected chemical scavenger. However, few studies aim to understand the role of active species in the degradation pathways and by-products generation to highlight the role of the ROS involved in the complete photocatalytic degradation process [34-38]. The intervention of ROS leading to the initial photoreaction process is not the same in all studies since the oxidation can proceed through different mechanisms. In this context, it is utmost importance to identify the main active species and determine their roles in the formation of intermediates in order to develop and understand the mechanisms underlying the reactivity of photocatalysts for environmental remediation [39]. Although some studies of ametryn degradation by photocatalysis have been reported [40-45], none of them investigated the role of reactive species involved in the degradation process and their role in the degradation pathways.

This work focused on the elucidation of the photocatalytic mechanism for the removal of ametryn by TiO_2 catalysts under simulated solar light. To achieve these objectives, studies were conducted to identify the main active species formed in the process using selected

chemical scavengers specific for $HO^{\bullet}$, $O_2^{\bullet-}$, $^1O_2$ and holes. In addition, a detailed study of the influence of each active species on the generation of degradation products and degradation pathways has been performed, in which the reaction intermediates were detected by means of exact mass measurements performed by liquid chromatography coupled to quadrupole-time of-flight mass spectrometry (LC-ESI-QTOF–MS/MS). The optimization of catalyst concentration was investigated considering the rate of ametryn removal. For this purpose, the parameters inherent to the process were evaluated such as TOC, COD, DBO, SUVA and the toxicity using Microtox® test. Besides the objective of mechanistic details of the photodegradation, the second-order rate constant of reaction between ametryn and $HO^{\bullet}$ radicals was calculated under optimal conditions.

2. Materials and methods

2.1.Chemicals

All chemicals used in the experiments were of analytical grade. Solutions of 10 mg L^{-1} of ametryn (CAS number: 834-12-8, purity 99.5%, $C_9H_{17}N_5S$, MW 227.33 g mol^{-1}, Sigma–Aldrich Chemical Co) were prepared using deionized water. The photocatalyst used (TiO_2 P25) was from Evonik Industries AG (Germany). Formic acid (85%), *tert*-butanol (99.7%), sodium azide (>99.5%) and 1,4-benzoquinone (>99%) were supplied by Probus S.A. (Spain), Panreac (Spain), Sigma–Aldrich Chemical Co and Merck (Germany), respectively. Acetonitrile was purchased from Fischer Chemical and orthophosphoric acid (85%) from Panreac Quimica.

2.2. Photocatalytic experiments

To perform the photocatalytic experiments under simulated sunlight, a solar simulator ((Solarbox, Co.fo.me.gra, 220 V, 50 Hz, see Fig. 1)) equipped with a 1000 W xenon lamp (Xe-OP, Phillips) was used. Within the solar simulator, a tubular reactor (Duran glass material, 24 cm length, 2.11 cm diameter, 0.078 L illuminated volume) was placed horizontally at the bottom under a parabolic mirror made of relative aluminum. An optical filter cutting off wavelengths under 280 nm was located just below the lamp. The photon flux arriving at the photoreactor was measured by o-nitrobenzaldehyde (o-NB) actinometry [46]. As can be seen in Fig. 1, the installation is also composed of a reservoir tank (total volume 1L), a peristaltic pump (Ecoline VC280 II, Ismatec) and a thermostatic bath (Haake K10) for carrying out experiments at a controlled temperature.

The experiments were carried out in the following steps: (i) First, 1 L of 10 mg L^{-1} ametryn solution (natural pH of the solution around 5.7) was introduced in a jacketed reservoir tank. (ii) Then, the amount of catalyst under study was added and different scavengers when needed. In this tank, the solution was magnetically stirred and maintained at constant temperature of 25 ºC with a thermostatic bath. (iii) The solution to be treated was continuously pumped into the photoreactor by peristaltic pump from the reservoir tank with a flow rate of 0.65 L min^{-1}. (iv) After 30 minutes of recirculation of the solution in the dark, the lamp was activated and began experiments lasting 120 minutes. Samples were collected at predetermined times throughout the reaction time, obeying a maximum of 10% withdrawal from the total volume. To remove the catalyst, before the analysis, samples were filtered with a polyethersulfone membrane filter of 0.45 µm. The experiments were conducted in triplicate to ensure reproducibility and mean values are reported.

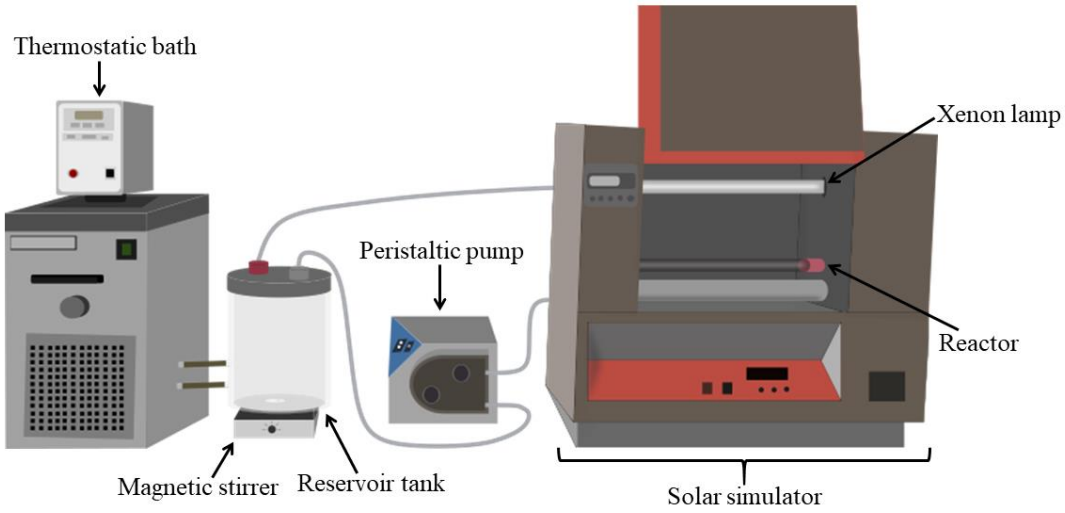

Fig. 1. Scheme of the solar simulator and experimental device.

2.3. Analytical Methods

The monitoring of the decrease in concentration of ametryn was carried out by high-performance liquid chromatography (HPLC) from Agilent 1200 Infinity Series using a SEA18 (5µm 15×0.46 cm from Teknokroma) and a Waters 996 photodiode array detector using the Empower Pro software 2002 Water Co. The mobile phase consisted of 78:22 (v/v) mixture of water (pH 3 adjusted by H_3PO_4) and acetonitrile, injected with a flow rate of 0.80 mL min^{-1} and detected at its maximum UV absorbance of 223 nm. In these parameters, the peak associated with ametryn appeared at 3.43 min, showing a limit of detection (LOD) = 0.018 mg L^{-1} and a limit of quantification (LOQ) = 0.055 mg L^{-1}.

The removal of total organic carbon (TOC) from the solutions subjected to the photocatalytic process was determined by a Shimadzu TOC-V CNS analyzer. The chemical oxygen demand (COD) was determined following the colorimetric method 5220D of Standard Methods for Examination of Water and Wastewater [47]. The colour of the sample was

measured in terms of the absorbance at 420 nm using a spectrophotometer (Hach Lange DR 2500) after digestion, employing 2 h of extreme catalytic oxidation conditions at 150 °C. The specific UV absorbance ($SUVA_{254nm}$) values were calculated dividing the absorbance of a sample at 254 nm by its COD value in the predetermined time ($SUVA = (UV_{254}/COD_t)\times100$). The biological oxygen demand ($BOD_{5,20}$) was determined with the protocol of Standard Methods 5210D [47] by respirometric process using OxiTop equipment during 5 days, under constant stirring and controlled temperature at 20 °C.

The potential toxicity of degradation by-products was measured by the Microtox® tests using a Model 500 Analyzer (Azur Environment, Workingham, England), which determines the inhibition of *Vibrio fischeri* bioluminescence. The toxicity was measured as the percentage of inhibition with respect to the light emitted after 15 min exposure. The analyzed data were expressed as toxicity units (equitox), $TU = [1/EC_{50}] \times 100$, where EC_{50} is the concentration which causes 50% of the light emission reduction.

To identify the by-products, samples collected from degradation experiments were analyzed by using an HPLC system (Agilent Series 1100, Agilent Technologies) connected to LC/MSDTOF (Agilent Technologies) mass spectrometer equipped with an electrospray ionization (ESI) interface operating in the positive ionization mode. The conditions used in the spectrometer were as follows: capillary 4000 V; nebulizer 15 psig; drying gas 7 L min^{-1}; gas temperature 325 °C; fragmentator 175 V; and HPLC conditions were the same as previously used to monitor degradation of ametryn. Spectra were acquired over the m/z 60–1200 range.

2.4. Effect of radical inhibitors

The role and contribution of $HO^{\bullet}$, $O_2^{\bullet-}$, h^+ and $^1O_2$, during the TiO_2 photocatalytic process, was investigated by adding well-known radical trapping reagents (scavengers) such as

tert-butanol (*t*-BuOH, 60 ml L^{-1}), 1,4-benzoquinone (BZ, 0.001 g L^{-1} corresponding to a molar relation of 1:10 for BZ:ametryn), formic acid (AcF, 0.82 mL L^{-1}) and sodium azide (NaN_3, 0.77 mg L^{-1}), respectively, in 10 mg L^{-1} ametryn solutions containing 0.4 g L^{-1} of catalyst. The concentrations of scavengers were based on previous research [34,46].

2.5. Determination of the second-order kinetic constant

To calculate the kinetic constant of the ametryn reaction by photocatalysis (considering only $HO^{\bullet}$ radicals), the competitive kinetic model was used. This procedure is applied assuming a general second order kinetics for the reaction between $HO^{\bullet}$ radical and the organic substance (OS), that is, first order in relation to the concentration of OS and first order in relation to the concentration of $HO^{\bullet}$ radicals [35]. Then, the removal rate of the OS can be expressed by the following Eq. (1):

$$\frac{\mathrm{d[OS]}}{\mathrm{dt}} = -k_{\mathrm{HO^{\bullet},OS}}[\mathrm{HO^{\bullet}}][\mathrm{OS}] \qquad (1)$$

Where [$k_{HO\bullet,OS}$] is the second order kinetic constant for the reaction between OS and $HO^{\bullet}$.

For the kinetic constant determination, competition kinetics method was applied. Simultaneous degradation experiments were performed with the mixture of the compound in study and a reference compound, whose rate constant for the reaction with $HO^{\bullet}$ radicals is previously known, which in this case was the 2,4-dichlorophenoxyacetic acid, 2,4-D ($k_{HO\bullet}$ = 5.5 x 10^9 L mol^{-1} s^{-1}) [48]. In this context, solutions containing both ametryn and 2,4-D with a

concentration of 0.04 mmol L^{-1} were subjected to photocatalytic degradation and their concentrations were followed with the time.

The concentration decay of the samples was monitored by HPLC from Agilent 1200 Infinity Series under the same conditions that were previously employed for monitoring the degradation of ametryn. 2,4-D was quantified at λ=234 nm. The data referring to the calibration curve for 2,4-D are the same as those presented in our previous study [49], which dealt with the determination of the second order kinetic constant between ametryn and $HO^{\bullet}$ by the UV/H_2O_2 process.

3. Results and discussion

3.1. Effect of TiO_2 concentration on ametryn degradation

The effect of the catalyst concentration on the ametryn removal response was evaluated, carrying out experiments with three different catalyst loads (0.05, 0.2 and 0.4 g L^{-1} TiO_2). These photocatalytic experiments were performed to find the concentration considered ideal for further investigate the role of active species in the mechanisms of the photocatalytic process. The results of the decay of the ametryn concentration and the removal of TOC are shown in Fig. 2. For both analyzed parameters, an increase in response is obtained when the catalyst dose is increased. The blank test shows that simulated sunlight with a photon flux equal to 9.4 μEinstein s^{-1} (290-400 nm) was insufficient to degrade ametryn, only around 30% of the herbicide was removed in 30 minutes of irradiation, not observing increased rate of degradation until the end of the experiment. Moreover, mineralization reached was insignificant, obtaining 6% after 120 minutes of irradiation. Among the concentrations of catalyst tested, using 0.4 g L^{-1} of TiO_2 leads to the best herbicide removal (100% removal after 60 min of irradiation) and

mineralization (>20% after 120 min of irradiation). Previous studies carried out with the same experimental installations [50] reported that, working with 0.5 g L^{-1} of TiO_2, catalyst sedimentation at the bottom of the reactor was observed, therefore concentrations greater than 0.4 g L^{-1} were not considered for the experiments. The TiO_2 settling in the reactor could increase radiation scattering, decreasing the reaction rate and masking the results of the experiments.

Degradation data were fitted to pseudo first-order kinetics model and the values obtained for the apparent first-order rate constant (k_{app}) were calculated from the slopes of the regression curves of the relationship between $-\ln([ametryn]/[ametryn]_0)$ and the irradiation time. It was clearly appreciated that kinetic constant decreases when TiO_2 concentration decreases, being k_{app} values 7.7 x 10^{-2} min^{-1} (R^2 = 0.997), 5.7 x 10^{-2} min^{-1} (R^2 = 0.978) and 5.3 x 10^{-2} min^{-1} (R^2 = 0.978), for 0.4, 0.2 and 0.05 g L^{-1} of TiO_2, respectively, which represented a good fit with for the proposed model. On the other hand, in the absence of the catalyst, the obtained value of k_{app} was 1.2 x 10^{-2} min^{-1} (R^2 = 0.995), roughly 6.4 times lower than for the experiments performed with 0.4 g L^{-1} of TiO_2.

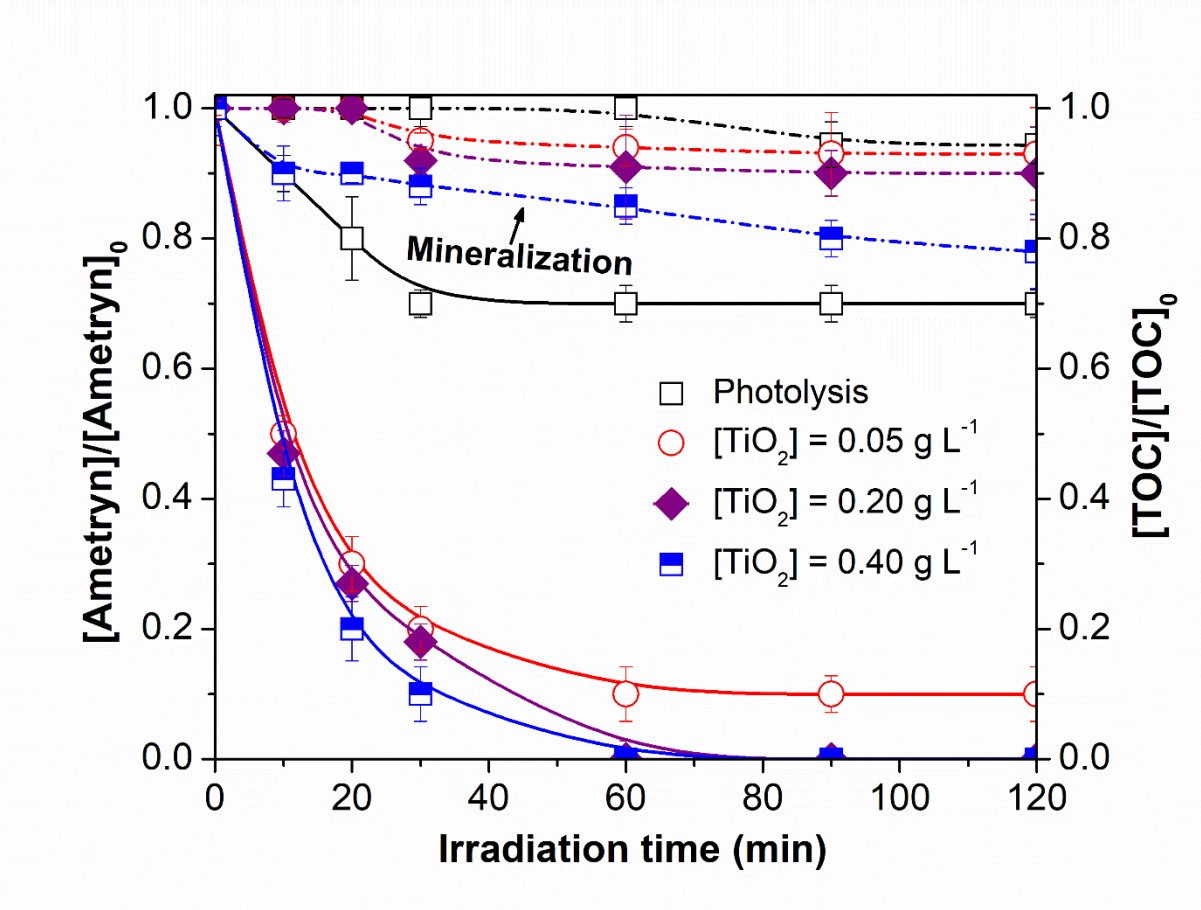

Fig. 2. Effect of the TiO_2 concentration on ametryn degradation and mineralization in solar simulator device. Initial ametryn concentration 10 mg L^{-1}, initial $pH_{free} \approx 5.7$.

3.2. Evolution of oxidation, aromaticity, toxicity and biodegradability assessment of intermediates

The removal of COD was evaluated during the photocatalytic process and the results with 0.4 g L^{-1} of catalyst are shown in Fig. 3A. The COD reduction found after 120 minutes of irradiation was around 60%. The COD is a parameter indicating the amount of organic matter in water sample, providing a direct correlation with C and O atoms in the molecular structure [51,52]. When the results are expressed as a correlation COD vs. time usually provides the S-shape curve [52]. When an inflection point is observed in this curve, it can be said that aliphatic

compounds begin to prevail over the aromatic compounds in the reaction mixture [52]. As can be seen from Fig. 3A, such inflection point was not observed during the experiment performed, indicating a considerable fraction of aromatics, resulting from the formation of intermediates derived from the s-triazine ring of the ametryn molecule.

Aromaticity, represented by SUVA, which indicates the correlation with aromatic organic matter content [53], was determined. These results are also presented in Fig. 3A (blue line in the graph). It is possible to observe an increase of the aromaticity with the increase of the degradation time, reaching a maximum value in 30 minutes of experiment. After 60 minutes there is a decrease in SUVA value, however at the end of the experiment, the value is still higher than the initial one. This indicates that the aromatic intermediates generated in the process were not completely degraded, which is in accordance with the low mineralization obtained (see Fig. 2).

Summarizing, the COD curve and the SUVA results show the presence of aromatic compounds in the system along all the process. These results agree with hydroxylated intermediates proposed for the degradation of ametryn by photocatalysis (see section 3.5.1.).

As pesticides are generally non-readily biodegradable and have high toxicity [54], the biodegradability and toxicity of samples subjected to degradation processes are important parameters that must be measured. The biodegradability index of ametryn solution before and after treatment was calculated as the ratio of $BOD_{5,20}$ to COD. The treated solution was considered biodegradable when this ratio was in the range of 0.4–0.8 [55]. Fig. 3B shows the effect of photocatalytic treatment on biodegradability index ($BOD_{5,20}$/COD ratio) improvement. The biodegradability index of the initial solution of ametryn was about 0.3, demonstrating that the ametryn solution is non-biodegradable. During the treatment period, the $BOD_{5,20}$/COD ratio steadily increases up to nearly 0.8 after 120 min of irradiation, suggesting that the hydroxylated intermediates formed are much more biodegradable.

Acute toxicity evolution before and after photocatalytic experiment, calculated by the light emission inhibition of *Vibrio fischeri*, is also shown in Fig. 3B. The initial equitox value of the untreated ametryn solution was nearly 8.6 and after the treatment was 0.25, that is, a reduction of around 97% of the toxicity was obtained. These results are in accordance with the increased biodegradability achieved through this treatment, possibly due to the lower toxicity of the hydroxylated intermediates formed during the treatment.

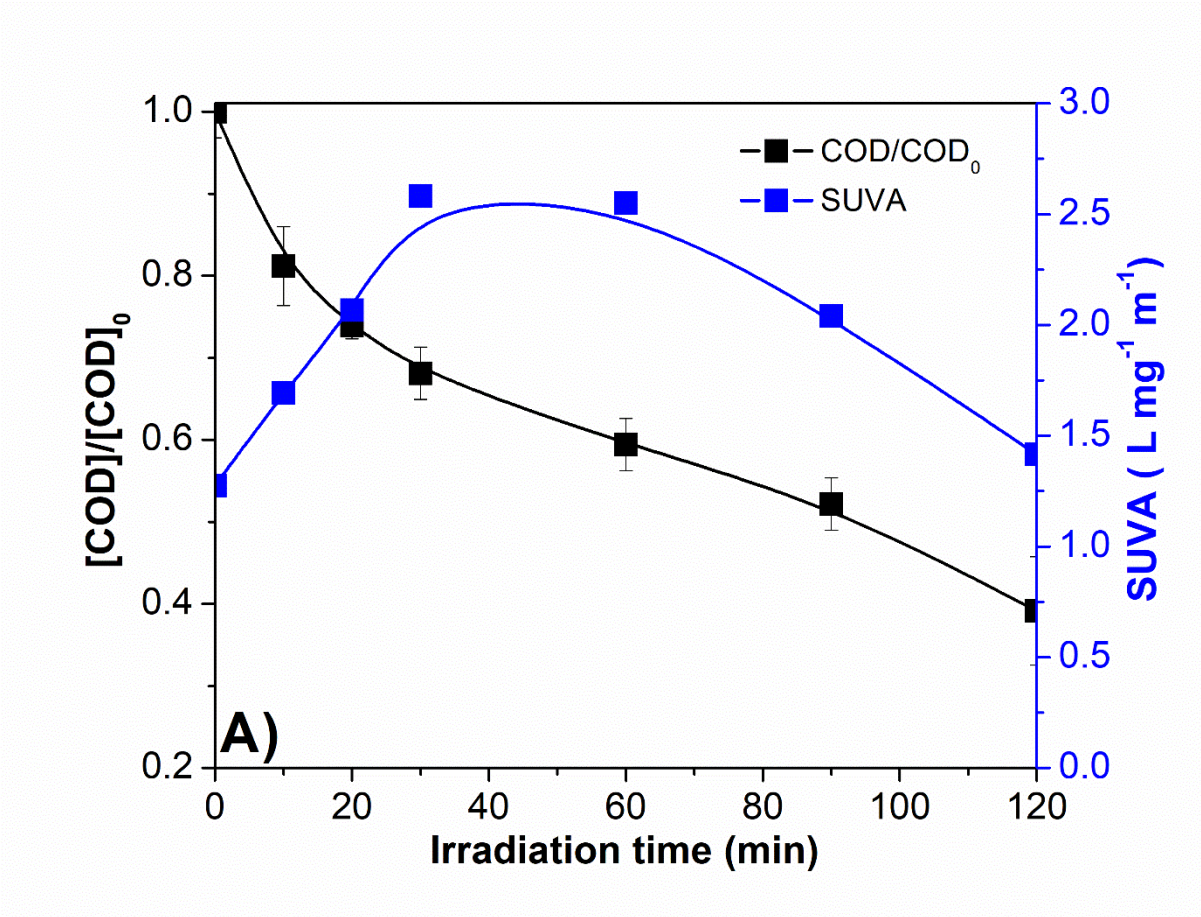

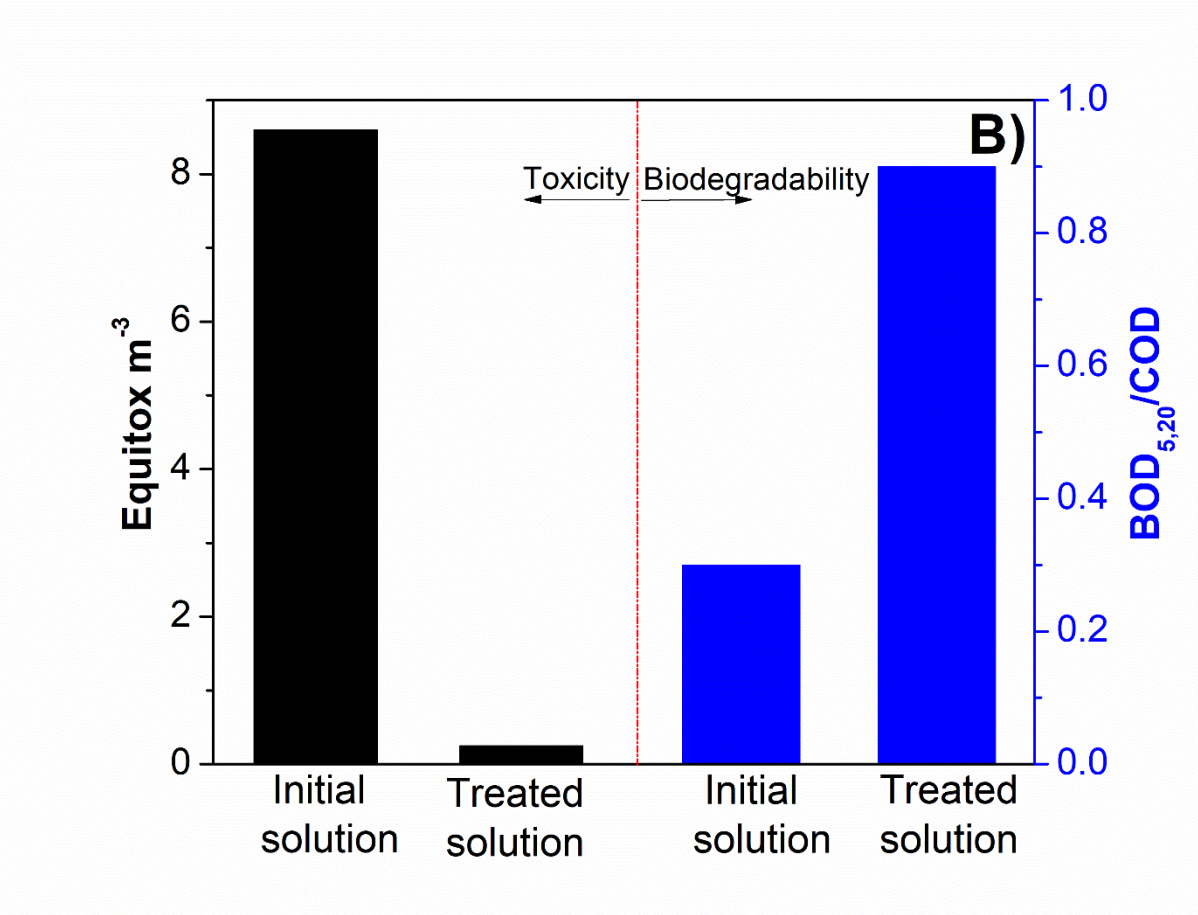

Fig. 3. (A) Oxidation (COD) and SUVA, (B) Biodegradability ($BOD_{5,20}$/COD) and Equitox for ametryn promoted by TiO_2 photocatalysis. $[Ametryn]_0$ = 10 mg L^{-1}, initial $pH_{free} \approx 5.7$, $[TiO_2]$ = 0.4 g L^{-1}.

3.3. Identification of the main reactive species involved in the photocatalytic degradation of ametryn

As previously reported, photocatalytic reactions involve the generation of various ROS. We utilized four selective radical scavengers to assess the extent of ametryn degradation provoked by $HO^{\bullet}$, $O_2^{\bullet-}$, $^1O_2$ and h_{BV}^+. The scavengers and their reactions with free radicals are summarized in Table 1.

The *t*-BuOH was reported to be a good scavenger of free $HO^{\bullet}$ radical [34,39,56]. The BZ is used to evaluate the contribution of $O_2^{\bullet-}$ radical [32,34]. However, BZ has also a great capacity to trap electrons at the surface of TiO_2 to form hydroquinone (HQ) [33,56]. The decrease of the number of electrons reduces the generation of $O_2^{\bullet-}$ and may then inhibit the rate of degradation due to the attack of this active specie [57].

AcF could significantly suppress the h_{BV}^{+} and $HO^{\bullet}$ radicals (free and adsorbed) in TiO_2 photocatalyst [33,34,58]. Sodium azide (NaN_3) is an efficient scavenger for the singlet oxygen produced by the interaction of $O_2^{\bullet-}$ radical and photo-generated h_{BV}^{+} [59,60]. Additionally, azide ions are also scavengers for $HO^{\bullet}$ radicals [38], as shown in Table 1.

The effect of these scavengers on the ametryn photodegradation rate is shown in Fig. 4. Table 1 also includes the inhibitory effect of each scavenger expressed as the percentage of decrease of the ametryn removal, as well as the percentage of contribution of each active species during the photocatalytic degradation of ametryn.

In BZ presence after 120 min of irradiation, there is only 3% inhibition on the elimination of the herbicide compared to the experiment in the absence of scavengers, suggesting that the $O_2^{\bullet-}$ radicals plays a minor role in the photocatalytic process. However, it is worth mentioning that the perhydroxyl radicals ($HO_2^{\bullet}$) may participate along with the radicals $O_2^{\bullet-}$ during the photocatalytic process. This occurs because these species are in equilibrium ($HO_2^{\bullet} \leftrightharpoons O_2^{\bullet-}$) and this equilibrium depends on the pH of the solution [61]. As the pKa value of this equilibrium is 4.7, it can be concluded that $O_2^{\bullet-}$ becomes the predominant species in solutions whose pH is 6 [61]. In this study, the pH of the ametryn solution was around 5.7 (below 6), the equilibrium can be displaced to the formation of the $HO_2^{\bullet}$ radicals, explaining the low inhibition rate in the presence of BZ.

In the presence of *t*-BuOH, the efficiency of ametryn degradation reduces from 100% to 18% after 120 min of experiment (*i.e.*, 82% inhibition in the rate of degradation was

observed). This suggests that free $HO^{\bullet}$ radicals were mainly implicated in ametryn degradation with TiO_2 P25. When AcF was added to the ametryn solution, an extensive inhibited in herbicide degradation was obtained. As shown in Fig. 4, only 12% removal was observed after 120 min of irradiation. As AcF is used to evaluate the participation of the hole and $HO^{\bullet}$ (free and adsorbed), the higher the rate of inhibition by means of the AcF in comparison to the inhibition by *t*-BuOH, the greater the direct participation of the hole (h_{BV}^{+}) in ametryn oxidation. These results (see Table 1) indicated that 88% of the degradation rate of ametryn was originated from both the $HO^{\bullet}$ radicals and h_{BV}^{+}. Thus, the contribution percentage of h_{BV}^{+} in the degradation rate was deduced as 6% by subtracting the percentage of $HO^{\bullet}$ radicals from the total percentage.

Azide, a scavenger for $HO^{\bullet}$ and $^1O_2$, also significantly reduced the degradation rate of ametryn (Fig. 4). When it was added, the rate of ametryn removal was 39% after 120 min of irradiation, *i.e.*, leading to 61% ametryn degradation inhibition. However, it is verified that this inhibition is smaller than that obtained by adding *t*-BuOH. If the contribution of $^1O_2$ were significant, it would be expected that the inhibition of the rate of degradation of ametryn in the presence of sodium azide to be greater than in the presence of *t*-BuOH, which only affects $HO^{\bullet}$ radicals [58,62]. The $^1O_2$ does not seem therefore to play a meaningful effect on the degradation of ametryn.

In summary, it can be seen that the $HO^{\bullet}$ free radicals are the predominant active species responsible for the major degradation of ametryn using TiO_2 P25 as catalyst, followed by direct oxidation via h_{BV}^{+}, and, at a minor extend, by the contribution of $O_2^{\bullet-}$ radicals.

Table 1 shows that values below 100% are found (more specifically 91%) by summation of the contribution percentages of each active species evaluated. This difference can be due to the amount of non-captured radicals such as other reactive oxygen species (ROS), among them, the $HO_2^{\bullet}$ radicals. However, the total contribution of these ROS not analyzed was

only 9%. Accordingly, it was possible to identify with a good level of confidence the participation of the main reactive species involved in the ametryn oxidation by photocatalysis, using TiO_2 P25 as a catalyst.

Table 1: Oxidizing species quenched, scavengers used, reactions involved, percentage of inhibition due to the scavengers, and the percentage of contribution of each active species during the photocatalytic degradation of ametryn using TiO_2 P25 as catalyst.

Scavenger	Reactive species	Reactions	Inhibitory effect (%)	Percentage of contribution (%)
tert-butanol (*t*-BuOH)	$HO^{\bullet}_{free}$	$(CH_3)_3COH + HO^{\bullet} \rightarrow (CH_2C(CH_3)_2OH)^{\bullet} + H_2O$ $k = 6.0\times10^8$ L mol^{-1} s^{-1} [63]	82%	82% ($HO^{\bullet}_{free}$)
1,4-benzoquinone (BZ)	$O_2^{\bullet-}$	$BQ + O_2^{\bullet-} \rightarrow BQ^{\bullet-} + O_2$ k = 0.9-1.0x10^9 L·mol^{-1} s^{-1} [56]	3%	3% ($O_2^{\bullet-}$)
	e_{BC}^- (electron)	$BQ + 2e_{BC}^- + 2H^+ \rightarrow HQ$ k =1.35x10^9 L·mol^{-1}s^{-1} [64]		
	h_{BV}^+ (hole)	$HCOO^- + 2\,h^+ \rightarrow CO_2 + H^+$		
formic acid (AcF)	$HO^{\bullet}$	$HCOO^- + HO^{\bullet} \rightarrow CO_2^{\bullet-} + H_2O$ k = 3.2 × 10^9 L·mol^{-1} s^{-1} [65]	88%	6% (h^+)
sodium azide (NaN_3)	$^1O_2$	$N_3^- + {}^1O_2 \rightarrow N_3^{\bullet} + O_2^{\bullet-}$ k = 2.0 × 10^9 L·mol^{-1} s^{-1} [58,62]	61%	-
	$HO^{\bullet}$	$N_3^- + HO^{\bullet} \rightarrow N_3^{\bullet} + HO^-$ k = 1.0 × 10^{10} L·mol^{-1} s^{-1} [62]		

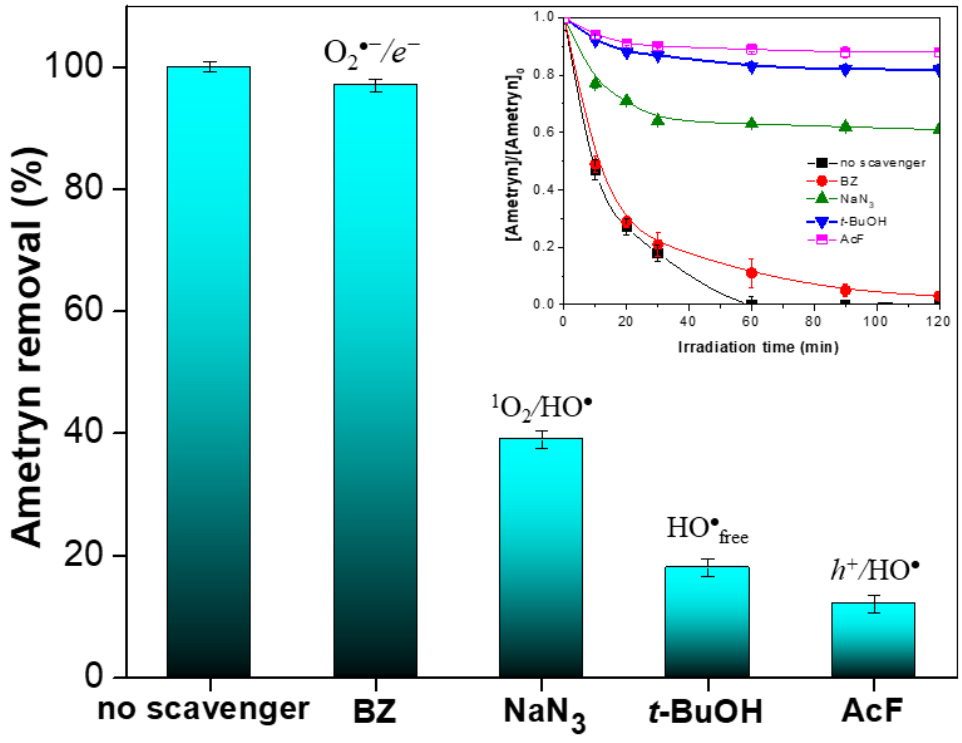

Fig. 4. Effect of different scavengers on ametryn removal efficiency using 0.4 g L^{-1} of TiO_2 catalysts under Xenon lamp at $pH_{free} \approx 5.7$. $[Ametryn]_0$ = 10 mg L^{-1}; [BZ] = 0.001 g L^{-1}; [AcF] = 0.82 mL L^{-1}; [NaN_3] = 0.77 mg L^{-1}; [*t*-BuOH] = 60 ml L^{-1}.

3.4. Estimation of the second-order kinetic constant between ametryn and the photo-generated HO• radicals by competition method

As the HO• radicals were the active species that played the most significant role in the photocatalytic degradation of ametryn (more than 80% removal was conducted by free HO• radicals), the next step was to determine the rate constants for the reaction between the herbicide and these radicals, by the application of the competition kinetics method.

The decay curve of the of the normalized concentrations of both ametryn and 2,4-D in the mixture over time is shown in Fig. 5A. This model is a way of solving the problems

encountered to measure the reaction rate of HO• radicals, due to the limitations of analytical techniques since reactions are very fast [66]. The model has been used successfully by several authors, such as, Dantas et al. [67], de Oliveira et al. [49], Zeghioud et al. [68], Ismail et al. [35], da Silva et al. [69].

The following equations can describe the removal rate of both ametryn and 2,4-D:

$$\frac{\mathrm{d}[2,4-\mathrm{D}]}{\mathrm{dt}} = -k_{\mathrm{HO}^\bullet,2,4-D}[\mathrm{HO}^\bullet][2,4\mathrm{D}] \qquad (2)$$

$$\frac{\mathrm{d}[\mathrm{Ametryn}]}{\mathrm{dt}} = -k_{\mathrm{HO}^\bullet,Ametryn}[\mathrm{HO}^\bullet][\mathrm{Ametryn}] \qquad (3)$$

Dividing Eq. (2) by Eq. (3) and integrating, Eq. (4) is obtained:

$$\ln\frac{[2,4-\mathrm{D}]}{[2,4-\mathrm{D}]_0} = -\frac{k_{\mathrm{HO}^\bullet,2,4-D}}{k_{\mathrm{HO}^\bullet,Ametryn}}\ln\frac{[\mathrm{Ametryn}]}{[\mathrm{Ametryn}]_0} \qquad (4)$$

According to Eq. (4), by plotting ln([2,4-D]/[2,4-D]$_0$) against ln([Ametryn]/[Ametryn]$_0$), as shown in Fig. 5B, a straight line (R^2 = 0.987) was obtained, whose slope is the ratio of rate constants. As the experimental points are satisfactorily arranged around the straight line, the goodness of the model used can be confirmed. After least square regression analysis, the ratio $k_{\mathrm{HO\bullet 2,4\text{-}D}}/k_{\mathrm{HO\bullet Ametryn}}$ was determined to be 11.6. Thus, the calculated value of $k_{\mathrm{HO\bullet Ametryn}}$ was 4.74 x 10^8 ± 0.29 x 10^7 L mol^{-1} s^{-1}. HO• quickly reacts with most pesticides through electron transfer with second-order rate constants varying between 10^7 and 10^{10} L mol^{-1} s^{-1} [70,71]. Therefore, the value found experimentally is in the range of most reactions of HO• with pesticides confirming that these radicals are the main reactive specie involved in ametryn oxidation by photocatalysis using TiO_2 P25 as a catalyst.

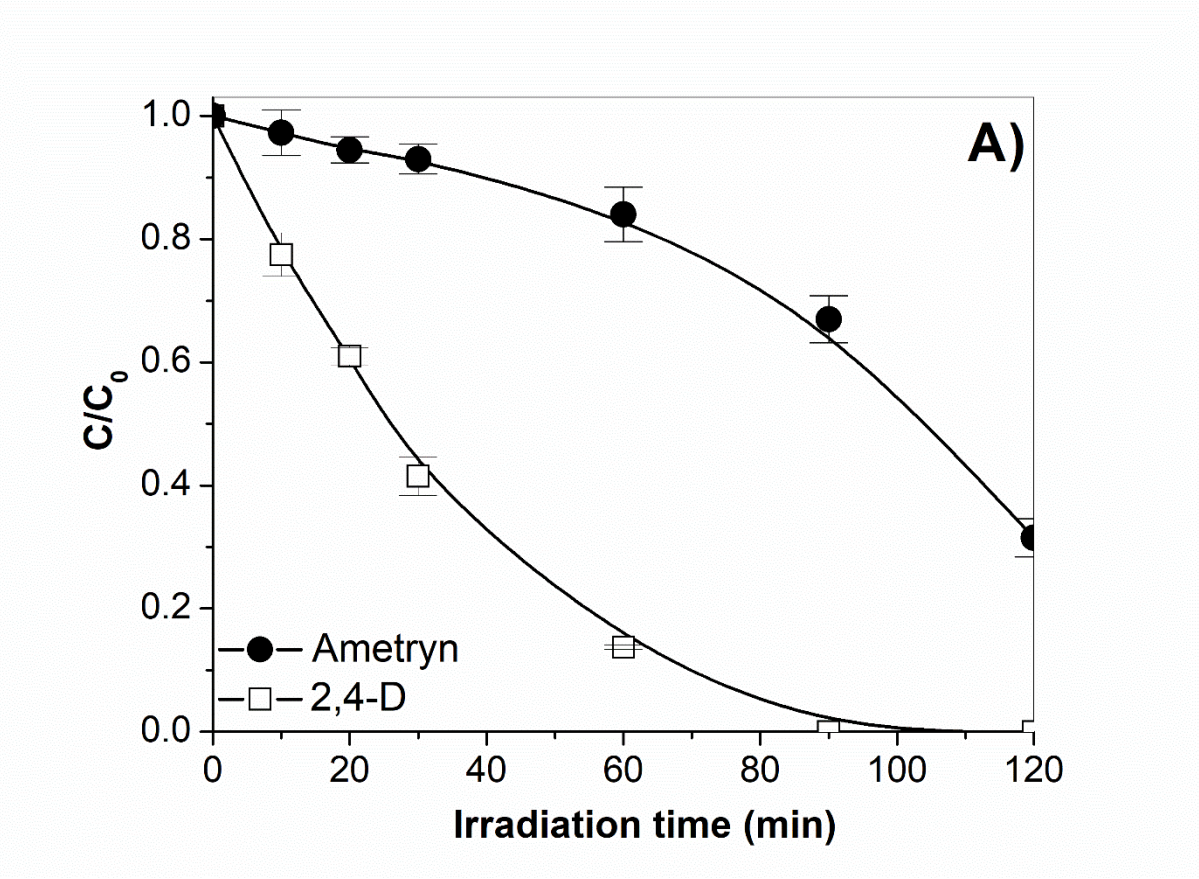
A)
C/C0
Irradiation time (min)
Ametryn
2,4-D
0.0
0.2
0.4
0.6
0.8
1.0
0
20
40
60
80
100
120

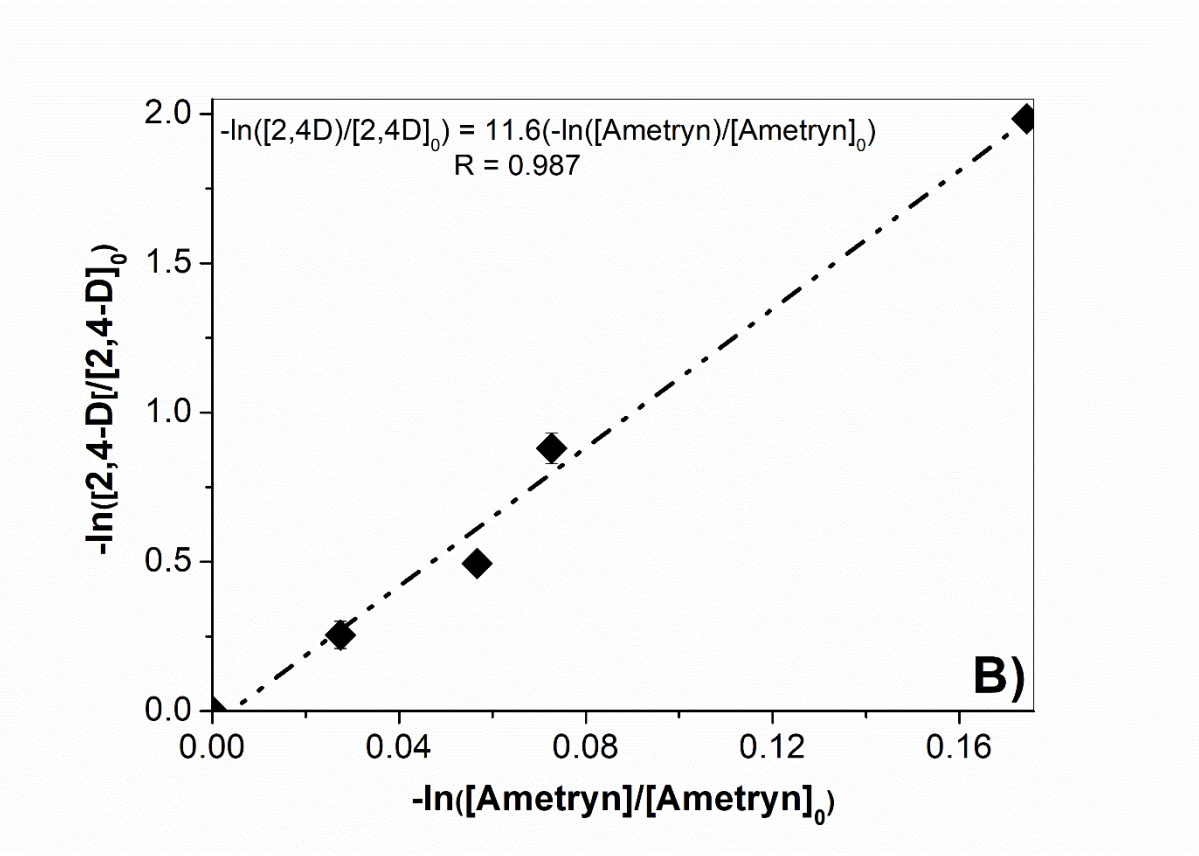
-ln([2,4D)/[2,4D]0) = 11.6(-ln([Ametryn)/[Ametryn]0)
R = 0.987
-ln([2,4-D[/[2,4-D]0)
-ln([Ametryn]/[Ametryn]0)
B)
0.0
0.5
1.0
1.5
2.0
0.00
0.04
0.08
0.12
0.16

Fig. 5. (A) Simultaneous degradation of ametryn and 2,4-D by photocatalysis, both at 0.04 mmol L^{-1}, [TiO_2] = 0.4 g L^{-1}, 25 °C, pH = 4.4 ± 0.2. (B) Neperian logarithms of the normalized concentrations of 2,4-D and ametryn for determination of second-order rate constant for the reaction between ametryn and $HO^{\bullet}$ radicals.

3.5. Degradation mechanism of ametryn: Relationship between the active species and the intermediates generated

For the identification and structural elucidation of intermediates generated during the photocatalytic treatment, samples collected at various treatment stages (10 min, 30 min and a final sample mixture at 120 min) were analyzed by LC-TOF-MS in positive ionization. The experiments were performed with 10 mg L^{-1} ametryn and 0.4 g L^{-1} TiO_2 in the absence and presence of the different scavengers studied.

Under the adopted conditions, a total number of thirty-eight intermediate products have been identified (with or without scavengers). Table 2 summarizes the abbreviations used for intermediates, with their analytical information including observed exact masses of protonated ions and empirical formula provided by the LC/MSD TOF ESI-TOF software. Table 2 also shows a comparison between the by-products generated in the degradation of ametryn with the addition of each scavengers investigated.

Table 2: LC/MS information of the by-products of ametryn solution after undergoing photocatalysis using TiO_2 without and with the addition of scavengers.

Abbreviation (Molecular ion (m/z), [M+ H^+])	Accurate mass of $[M+H]^+$	Molecular formula	Occurrence				
			TiO_2	TiO_2 + BZ	TiO_2 + *t*-BuOH	TiO_2 + AcF	TiO_2 + Azide
228	228.1271±1.30x10^{-4}	Ametryn ($C_9H_{17}N_5S$)	Y	Y	Y	Y	Y
105	104.9904	$C_2H_4N_2O_3$	N	N	N	N	Y
116	116.0258	$C_3H_9N_5$	N	N	Y	N	N
127	127.0706	$C_3H_6N_6$	N	N	N	Y	N
132	131.9596	$C_3H_9N_5O$	N	N	Y	N	N
144	144.0569±2.12x10^{-4}	$C_4H_5N_3SO$	N	Y	Y	N	N
146	146.0174	$C_3H_7N_5O_2$	N	N	N	N	Y
156	155.9725	$C_4H_5N_5S$	N	N	Y	N	N
158	158.0409	$C_4H_7N_5S$	N	Y	N	N	N
159	158.9943	$C_4H_6N_4SO$	Y	N	N	N	N
164	163.9673	$C_3H_5N_3SO_3$	N	Y	N	N	N
165	165.0116	$C_4H_8N_2SO_3$	N	N	N	N	Y
174	173.9846	$C_4H_7N_5SO$	N	N	Y	N	N
175	174.9670	$C_4H_6N_4SO_2$	Y	N	N	N	N
182	181.9777	$C_6H_7N_5S$	N	Y	N	N	N
186	186.0795±1.29x10^{-4}	$C_6H_{11}N_5S$	Y	Y	Y	Y	N
187	186.9941	$C_6H_{10}N_4SO$	N	N	N	N	Y
198	198.1337	$C_7H_{11}N_5S$	N	Y	N	N	N
200	200.0951±2.081666x10^{-4}	$C_7H_{13}N_5S$	Y	Y	Y	N	N
214	214.1116	$C_7H_{11}N_5SO$	N	Y	N	N	N

216	215.9950	$C_7H_{13}N_5SO$	N	N	Y	N	N
219	219.0162	$C_6H_{10}N_4SO_3$	Y	N	N	N	N
236	235.9938±5.798276x10^{-3}	$C_5H_9N_5SO_4$	Y	N	Y	N	N
238	238.0104	$C_4H_7N_5SO_5$	Y	N	N	N	N
240	239.6648±0.5178851	$C_9H_{13}N_5SO$	Y	Y	Y	Y	N
242	242.1261±1.980387x10^{-2}	$C_9H_{15}N_5SO$	Y	Y	Y	Y	N
243	243.1109	$C_9H_{16}N_5SO$	N	Y	N	N	N
244	244.1207±1.457166x10^{-2}	$C_9H_{17}N_5SO$	Y	Y	N	Y	N
246	246.0168	$C_8H_{15}N_5SO_2$	N	N	N	Y	N
250	250.1089±3.768289x10^{-4}	$C_6H_{11}N_5SO_4$	Y	Y	Y	Y	Y
254	254.0014±1.414214x10^{-4}	$C_4H_7N_5SO_6$	Y	N	N	N	Y
260	259.9986	$C_8H_{13}N_5SO_3$	N	N	N	Y	N
262	262.0590	$C_8H_{15}N_5SO_3$	N	N	Y	N	N
264	264.0875± 1.414214x10^{-3}	$C_7H_{13}N_5SO_4$	Y	Y	N	N	N
266	266.1027	$C_6H_{11}N_5SO_5$	N	Y	N	N	N
278	278.0388	$C_7H_{11}N_5SO_5$	Y	N	N	N	N
351	351.0025	$C_9H_{18}N_8SO_5$	N	N	N	N	Y
411	411.0068	$C_{14}H_{22}N_{10}S_2O$	N	N	N	N	Y
433	433.0060	$C_{11}H_{16}N_{10}S_2O_5$	N	N	N	N	Y

Yes (Y) or Not (N)

Fig. S1 (supplementary material) reports a mass spectrum model with the formed intermediates at *m/z* 159, 175, 186, 200 and 219, corresponding to ametryn solutions irradiated with TiO_2 particles in the absence of scavengers. The molecular structures defined for the by-products are shown in Fig. S2.

In this section, a discussion was first conducted addressing the intermediates generated in the photocatalytic process without scavengers. Subsequently, the generation of intermediates was evaluated with the addition of different scavengers. All these data allowed us to propose a mechanism for ametryn degradation shown in Fig. 8.

3.5.1. Identification of by-products structures during photocatalytic reaction without addition of scavengers

Fig. 6 presents a scheme with fourteen intermediate products identified in the TiO_2 process with *m/z* 159, 175, 186, 200, 219, 236, 238, 240, 242, 244, 250, 254, 264 and 278. The formed intermediates with *m/z* 186, *m/z* 200, *m/z* 244 are common by-products of ametryn oxidation, as identified in our previous study [49] and also by other researchers. Chen et al. [72], Jiang et al. [73] and Yang et al. [74] found in their studies degradation products for ametryn with the same *m/z* 186 and *m/z* 200. The intermediate with *m/z* 200 was also proposed by Gozzi et al. [75] for the degradation of ametryn by solar photoelectro-Fenton, as well as a metabolite generated from biodegradation of the herbicide by entomopathogenic fungal cosmopolite *Metarhizium brunneum* ARSEF 2107 [11]. The intermediate with *m/z* 244 was also identified by Lopez et al. [76] and Mascolo et al. [77] in the degradation of ametryn by means of sodium hypochlorite and chlorine dioxide disinfectants, and by Yang et al. [74] during the UV/chlorine process. Liu et al. [78] proposed this intermediate in the heterogeneous reaction of ametryn particles with NO_3 radicals.

In our previous study of ametryn degradation by homogeneous oxidative processes [49], we identified the intermediate with *m/z* 240 and proposed the same structure as presented in this study. On the other hand, particular attention should be given to the formation of compounds of *m/z* 159, 175, 219, 236, 254, 264 and 278, as to the best of our knowledge, they have not been identified so far.

With the exception of intermediates with *m/z* 186 and *m/z* 200, all other by-products generated in the photocatalytic process are hydroxylated compounds, derived from sustained $HO^{\bullet}$ radicals attacks on sulfur in the R–S–CH_3 bond and/or the aliphatic part of the ametryn molecule.

The hydroxylation of the group (R-S-CH_3) led to the formation of sulphoxides (R-SO-CH_3) with *m/z* = 244, 242 and 240. Successive attacks by $HO^{\bullet}$ on aliphatic carbon chains of these intermediates resulted in hydroxylated by-products of lower molecular weight with *m/z* 219, 175 and 159 owing to the rupture of the aliphatic part of the sulphoxides.

Sulphones (R–SO_2–CH_3) with *m/z* 236, 250, 264 and 278 were detected as intermediates, resulting from the addition of an oxygen atom to the sulfur atom of by-product with *m/z* 244, and subsequent attacks by $HO^{\bullet}$ on alkylamino lateral chain, forming carboxylic acids and alcohols in the aliphatic part.

The attack of the $HO^{\bullet}$ radical on the generated sulfone (intermediate with *m/z* 236) led to the formation of by-products with the sulphonic acid group (R–$S(=O)_2$–OH). In this way, the inedited by-products, with mass peaks at *m/z* 238 and *m/z* 254, were proposed on basis of the formation of sulphonic acid group. The degradation by-product *m/z* 200 could come from the deethylation of ametryn molecule. Additionally, the by-product *m/z* 200 underwent further demethylation to produce the intermediate with *m/z* 186.

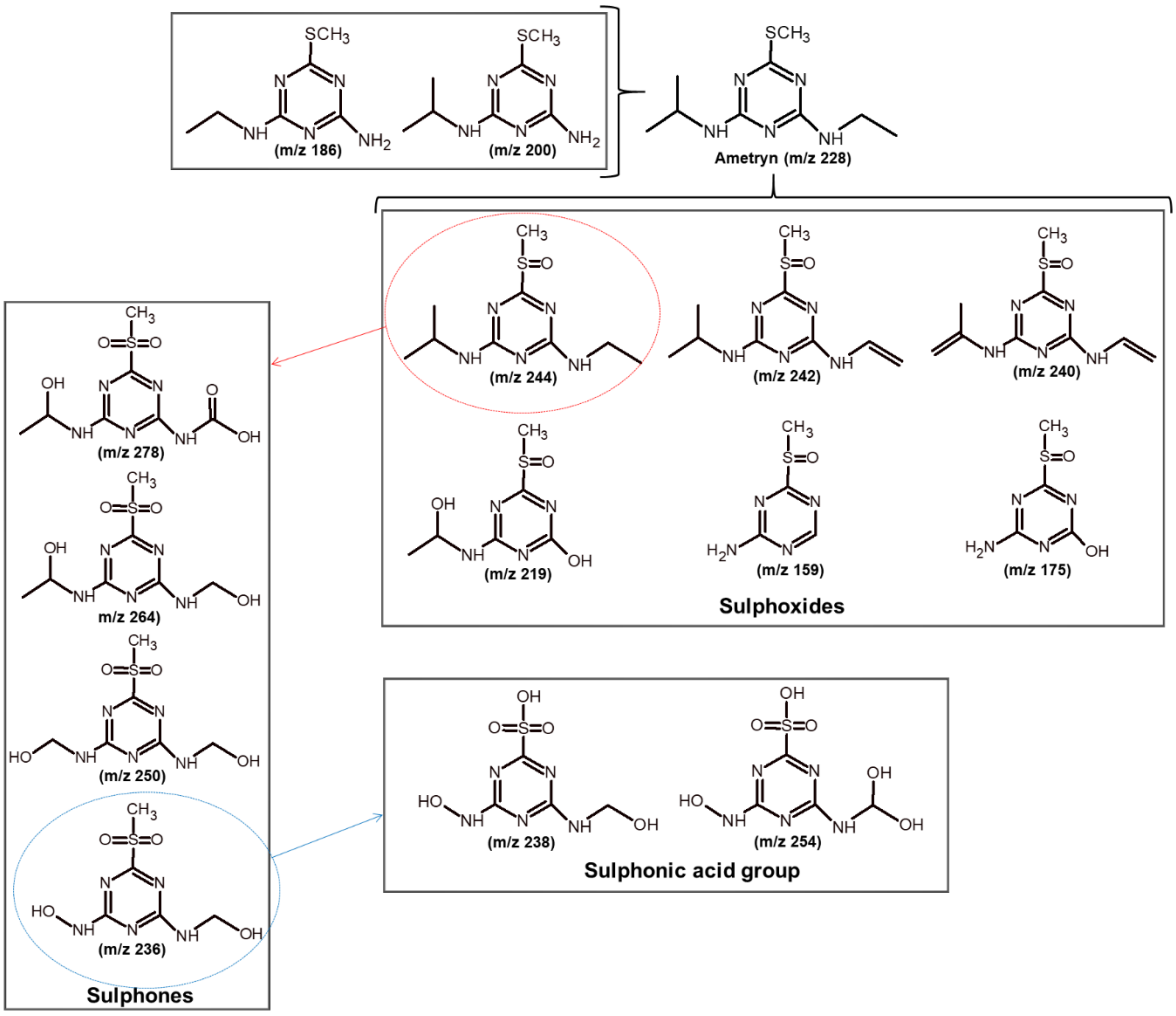

Fig. 6. Molecular structures of intermediates formed upon demethylation, deethylation and hydroxylation processes, proposed for the degradation of ametryn during photocatalytic treatment using TiO_2 P25 as catalyst.

3.5.2. Evolution of by-products generated in ametryn degradation in the presence of scavengers

3.5.2.1. Effect of $O_2^{\bullet-}$ and e_{BC}^- scavengers

In the ametryn degradation containing BZ, a total of fifteen intermediates were elucidated at *m/z* 144, 158, 164, 182, 186, 198, 200, 214, 240, 242, 243, 244, 250, 264, and 266, indicating that although inhibition of $O_2^{\bullet-}$ radicals generation occurs, there is a predominance of $HO^{\bullet}$ radicals.

Correlating the intermediates generated in this process with the experiment performed with the catalyst alone and/or several experiments with other scavengers, it is said that the by-products at *m/z* 158, 164, 182, 198, 214, 243 and 266 were generated only with the addition of BZ (see Table 2 and Fig. S2 in the supplementary material). In this process the main paths involved in the generation of intermediaries can be compiled in the sequential attack of $HO^{\bullet}$ radicals on the sulfur atom of the methylthio group in the ametryn molecule; by cleavage of the alkylamino lateral chain and by abstracting hydrogen from the alkylamino group, leading to the formation of double and triple bonds.

Intermediate identified with *m/z* 158 is a common by-product of ametryn degradation, as proposed by de Oliveira et al. [49], Chen et al. [72] and Liu et al. [78]. The intermediates with m/z 182, m/z 198 and m/z 266 were also identified in our previous study [49]. It is noteworthy that the intermediates with *m/z* 164, 214 and 243 were not found in the literature for other ametryn degradation studies.

3.5.2.2. Effect of $HO^{\bullet}$ scavengers

As previously discussed, (section 3.3), the ametryn removal significantly lessened with the addition of *t*-BuOH, indicating that $HO^{\bullet}$ mediated oxidation processes are the predominant vias by conventional TiO_2 photocatalysis under xenon lamp irradiation. Analysis by LC–MS-TOF allowed the identification of thirteen intermediates during ametryn photocatalytic degradation with the addition of the alcohol as shown in Table 2 and Fig. S2. Specifically, in this case the generated by-products presented mass peaks at *m/z* 116, 132, 144, 156, 174, 186, 200, 216, 236, 240, 242, 250 and 262. The presence of these intermediates generated with little or no participation of $HO^{\bullet}$ radicals, also demonstrates that the degradation of ametryn is driven by the participation of other active species such as $O_2^{\bullet-}$ radicals and direct oxidation via holes.

The intermediates formed in this case are markedly different. Comparing with intermediates reported only in the presence of catalyst or with the addition of other sequestering agents, 6 specific different intermediates were identified in the presence of *t*-BuOH. These products exhibiting $[M+H]^+$ ions at *m/z* 116, 132, 156, 174, 216 and 262 (see Table 2) and their proposed molecular structures are presented in Fig. S2 (see supplementary material). Apart from the intermediate with m/z 216 that was identified in our previous study [49], these other intermediates have not been identified so far. This finding suggests that $O_2^{\bullet-}$ and holes are also involved in the degradation process, however their role is less important.

Ring opening might occur via subsequent addition of $HO_2^{\bullet}$ radical/$O_2^{\bullet-}$ anion [34,79,80]. The identified by-products, with mass peaks at *m/z* 116 and *m/z* 132, are characterized by the opening s-triazine ring.

The attack of $O_2^{\bullet-}$ radicals on the sulfur atom of the methylthio group, followed by the breakdown of C-N single bonds between the s-triazine ring and isopropyl groups of the ametryn molecule, generated the sulphoxides with *m/z* 174 and *m/z* 216. It was also verified the

generation of a hydroxy sulphone with *m/z* 262, as the result of the $O_2^{\bullet-}$ radical attacks on the sulfur atom and via hydroxylation by $O_2^{\bullet}$ in the ethylamine part. The abstraction of hydrogen corresponding to methylthio group by reactions involving $O_2^{\bullet-}$ radicals and/or holes formed the intermediate with *m/z* 156.

3.5.2.3. Effect of holes and $HO^{\bullet}$ scavengers

When AcF was added to the reaction system, only eight intermediates with *m/z* 127, 186, 240, 242, 244, 246, 250 and 260 were identified by LC-TOF-MS analysis in positive mode (Table 2). In this case the degradation was mainly conducted by $O_2^{\bullet-}$ radicals and $^1O_2$ since $HO^{\bullet}$ radicals and h_{BV}^+ do not participate (or the participation is drastically reduced) in the presence of AcF (see section 3.3).

The intermediates with *m/z* 240, 242, 244 and 250 can be generated by the addition reaction of $O_2^{\bullet-}$ radicals on the sulfur atom and/or alkyl chain and by oxidation of alkyl chain. On the other hand, *m/z* 186 and *m/z* 127 are formed via the oxidation of the alkyl substituent with the stepwise decomposition of methyl, ethyl and isopropyl groups. From these intermediates generated, the by-product with *m/z* 127, 246 and 260 were formed only in the presence of AcF (Table 2 and Fig. S2) and to the best of our knowledge was not found in the literature in studies on ametryn degradation. Similarly, the intermediate with *m/z* 260 was also identified in our previous study [49]. However, we here propose a different structure for this intermediate, based on an ene reaction with singlet oxygen via the electron richer Nisopropyl group [81-84]. The Fig. 7 shows a proposed mechanism involved in the formation this by-product and for the formation of the *m/z* 246. These results suggest that $^1O_2$ initially may have participated in the degradation process, although from the results shown in Table 1, no

percentage contribution of ametryn degradation was attributed to $^1O_2$, because the predominance of HO• radicals can mask the process.

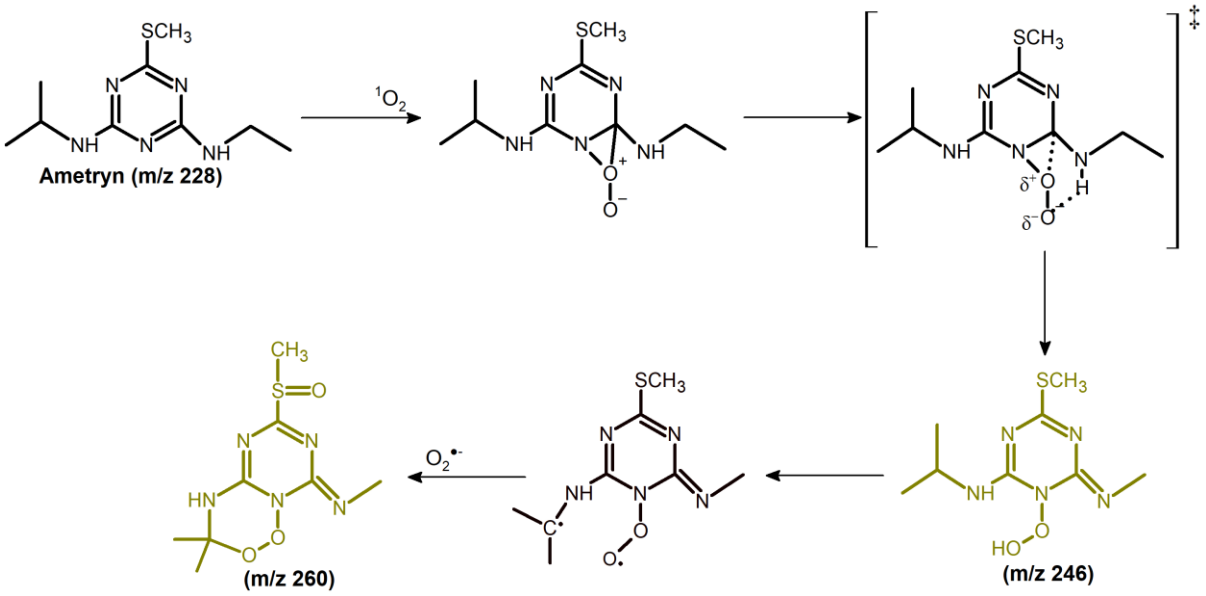

Fig. 7. Proposed mechanisms for the formation of by-produts at m/z 246 and m/z 260 resulting from photodegradation of ametryn by comercial TiO_2 catalyst in aqueous solution with addition of AcF.

3.5.2.4. Effect of $^1O_2$ and HO• scavengers

A total of nine intermediates were detected for the degradation of ametryn in experiments performed with the addition of azide. Table 2 shows that, in the presence of azide, they appear intermediates generated in the presence of other active species (with *m/z* 250 and 254), but new seven intermediates were also generated (with *m/z* 105, 146, 165, 187, 351, 411 and 433) that were not detected in the other cases.

As azide scavenges both, HO• radicals and $^1O_2$, the intermediates generated may result from the attack of $O_2^{\bullet-}$ radicals and direct oxidation via holes. However, it has also to take into

account the possible intermediates produced by activity of azidyl radical ($N_3^{\bullet}$), which is highly oxidative species [85], and/or by the extra amount of $O_2^{\bullet-}$ generated during the $^1O_2$ scavenging process (see Table 1).

The intermediates with *m/z* 105, 146 and 165 result from cleavage s-triazine ring, possibly via addition of $O_2^{\bullet-}$ radicals. The intermediate with *m/z* = 105 was also identified in our previous study [49], but the intermediates with *m/z* 146, 165, 187, 351, 411 and 433, to the best of our knowledge, have not been described in other studies of ametryn degradation.

Products resulting from dimerization can be generated by condensation reactions. Three intermediates identified with *m/z* 351, *m/z* 411 and *m/z* 433 are dimeric species.

3.5.3. Comparison of the same by-products generated with and without addition of the different scavengers.

Table 2 shows a comparison of the by-products that are repeated for the different analyzed processes. The sulphone at *m/z* 250 was detected in all cases investigated (with different scavenger and non-scavenger systems). The intermediates with *m/z* 186, 240 and 242 were not only identified in the experiment performed with azide. These by-products are the main products of photocalytic degradation of ametryn and can be generated by the attack of the different ROS. Other typical by-products of ametryn degradation already identified by other researchers and identified in this study (see Table 2) were the intermediates with *m/z* 200 and *m/z* 244.

The sulphones with *m/z* 236 and *m/z* 264 were both detected in the absence of scavengers, and the sulphone of *m/z* 236 was also detected with the addition of *t*-BuOH; in contrast to sulfone with *m/z* 264 was formed in the presence of BZ. Thus, it can be assumed

that the sulphone with *m/z* 236 was generated by $O_2^{\bullet-}$ radicals attack, and the sulphone with *m/z* 264 was generated via $HO^{\bullet}$ radicals.

The intermediate at *m/z* 254 with the sulphonic acid group was generated in the experiment performed in absence of scavengers and in the experiment with azide. The sulphoxide of low molecular weight at *m/z* 144 was identified for the experiment performed in the presence of BZ and *t*-BuOH. Thus, the formation of these by-products may involve $HO^{\bullet}$ or $O_2^{\bullet-}$ radicals.

Simulated solar radiation-induced TiO_2 photocatalysis involves the formation of different active species responsible for the formation of by-products resulting from degradation of ametryn. Therefore, the reaction pathway of the ametryn photocatalytic degradation catalyzed via commercial TiO_2 with main contributed ROS can be proposed in the scheme shown in Fig. 8.

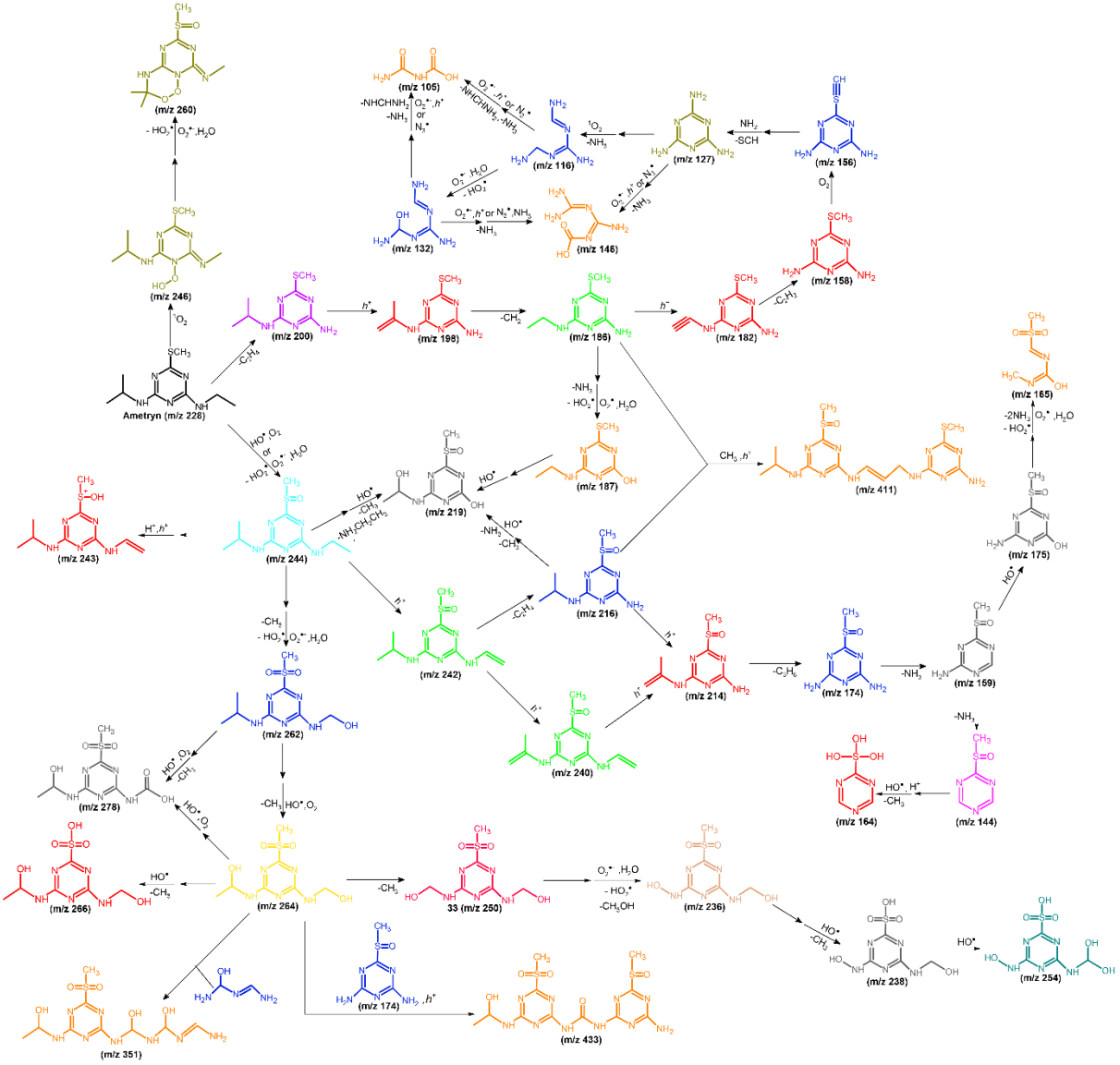

Fig. 8. Mechanisms postulated showing the proposed pathways for the photocatalytic degradation of ametryn by commercial TiO_2 catalyst via the dominate ROS involved in the process.

4. Conclusions

The most remarkable conclusions drawn for the present study can be summarized as follows:

- The photocatalysis using TiO_2 P25 as catalyst is proved to be efficient process for the degradation of ametryn herbicide in aqueous solutions under simulated solar radiation.

Using 0.4 g L^{-1} of catalyst, a complete ametryn degradation was reached after 60 min of experiment.

- Photocatalytic oxidation of ametryn significantly increased the biodegradability by a factor of around 2.7, making the final solution biodegradable. The toxicity assessment with *Vibrio fischeri* revealed that the degradation process eliminates virtually the toxicity and no toxic intermediates were formed at the end of the treatment.
- Experimental evidence obtained with radicals and hole scavengers indicates that the $HO^{\bullet}$ free radicals have a preponderant participation in the oxidation of ametryn with a high second order rate constant ($4.74 \times 10^8 \pm 0.29 \times 10^7$ L mol^{-1} s^{-1}), followed by direct hole ametryn oxidation. Also, a slight contribution in the oxidation can be attributed to $O_2^{\bullet-}$ anions species.
- The role of active species in the generation of intermediates has been systematically studied. From the by-products formed, it can be observed that the $HO^{\bullet}$ radicals primarily leads to the formation of sulphones, sulphoxides and sulphonic acid, produced by the sequential attack of $HO^{\bullet}$ radicals on the sulfur atom on the methylthio group. Meanwhile, $O_2^{\bullet-}$ can attack ametryn to form the open-s-triazine ring products, besides forming sulphoxides and hydroxy sulphones resulting from the attack of $O_2^{\bullet-}$ radicals on the sulfur atom. The oxidation of ametryn by $^1O_2$ leads to the formation of N-hydroperoxy specie and cyclohydroperoxy hemiaminal intermediate, arising from the participation in an ene type reaction with $^1O_2$ via the electron richer N-isopropyl group. Finally, the direct attack by positive holes can lead to compounds resulting from dimerization products by condensation reactions. These results offered an insight into the degradation mechanism of ametryn involving several active species.

Acknowledgements

The authors wish to thank the Brazilian funding agencies: Coordenação de Aperfeiçoamento de Pessoal de Nível Superior (Capes, Finance Code 001); Conselho Nacional de Desenvolvimento Científico e Tecnológico (CNPq); Fundação de Amparo à Pesquisa do Estado de São Paulo (FAPESP 2019/26210-8), Fundação de Apoio ao Desenvolvimento do Ensino, Ciência e Tecnologia do Estado de Mato Grosso do Sul (Fundect). The authors also thank the Ministry of Science and Innovation of Spain (projects CTQ2014-52607-R and CTQ2017-86466-R - MINECO/FEDER, UE) and AGAUR – Generalitat de Catalunya (projects 2014SGR245 and 2017SGR-131) for funds received to carry out this work.

References

[1] T. Bashnin, V. Verhaert, M. De Jonge, L. Vanhaecke, J. Teuchies, L. Bervoets, Relationship between pesticide accumulation in transplanted zebra mussel (Dreissena polymorpha) and community structure of aquatic macroinvertebrates, Environ. Pollut. 252 (2019) 591-598. https://doi.org/10.1016/j.envpol.2019.05.140.

[2] M. Bilal, H.M.N. Iqbal, D. Barceló, 2019. Persistence of pesticides-based contaminants in the environment and their effective degradation using laccase-assisted biocatalytic systems. Sci. Total. Environ. 695, 133896. https://doi.org/10.1016/j.scitotenv.2019.133896.

[3] W. McCance, O.A.H. Jones, M. Edwards, A. Surapaneni, S. Chadalavada, M. Currell, Contaminants of Emerging Concern as novel groundwater tracers for delineating wastewater

impacts in urban and peri-urban areas, Water Res. 146 (2018) 118-133. https://doi.org/10.1016/j.watres.2018.09.013.

[4] O.M. Rodriguez-Narvaez, J.M. Peralta-Hernandez, A. Goonetilleke, E.R. Bandala, Treatment technologies for emerging contaminants in water: A review, Chem. Eng. J. 323 (2017) 361–380. http://dx.doi.org/10.1016/j.cej.2017.04.106.

[5] S. Chiron, A.R. Fernandez-Alba, A. Rodriguez, E. Garcia-Calvo, Pesticide chemical oxidation: state-of-the-art, Water Res. 34 (2000) 366–377. https://doi.org/10.1016/S0043-1354(99)00173-6.

[6] S. Wang, Y. She, S. Hong, X. Du, M. Yan, Y. Wang, Y. Qi, M. Wang, W. Jiang, J. Wang, Dual-template imprinted polymers for class-selective solid-phase extraction of seventeen triazine herbicides and metabolites in agro-products. J. Hazard. Mater. 363 (2019) 686-693. https://doi.org/10.1016/j.jhazmat.2018.12.089.

[7] N. Rodríguez-González, M-J. González-Castro, E. Beceiro-González, S. Muniategui-Lorenzo, Development of a matrix solid phase dispersion methodology for the determination of triazine herbicides in marine sediments, Microchem. J. 133 (2017) 137–143. http://dx.doi.org/10.1016/j.microc.2017.03.022.

[8] H. Prosen, Fate and Determination of Triazine Herbicides in Soil, in: M.N.A.E-G. Hasaneen (Ed.), Herbicides - Properties, Synthesis and Control of Weeds, IntechOpen, 2012, pp. 43-58. DOI: 10.5772/33164. Available from: https://www.intechopen.com/books/herbicides-

properties-synthesis-and-control-of-weeds/fate-and-determination-of-triazine-herbicides-in-soil.

[9] A.C. Borges, M. do Carmo Calijuri, A.T. de Matos, M.E.L.R. de Queiroz, Horizontal subsurface flow constructed wetlands for mitigation of ametryn-contaminated water, Water SA 35 (2009) 441-445. http://www.wrc.org.za/.

[10] J. Shah, M.R. Jan, B. Ara, F.U. Shehzad, Determination of ametryn in sugarcane and ametryn–atrazine herbicide formulations using spectrophotometric method, Environ. Monit. Assess. 184 (2012) 3463–3468. https://doi.org/10.1007/s10661-011-2200-x.

[11] R. Szewczyk, A. Kuśmierska, P. Bernat, Ametryn removal by metarhizium brunneum: Biodegradation pathway proposal and metabolic background revealed, Chemosphere. 190 (2018) 174-183. https://doi.org/10.1016/j.chemosphere.2017.10.011.

[12] I. Ali, Z.A. AL-Othman, A. Alwarthan, Green synthesis of functionalized iron nano particles and molecular liquid phase adsorption of ametryn from water, J. Mol. Liq. 221 (2016) 1168–1174. http://dx.doi.org/10.1016/j.molliq.2016.06.089.

[13] G.B. Mahesh, B. Manu, 2019. Removal of ametryn and organic matter from wastewater using sequential anaerobic-aerobic batch reactor: A performance evaluation study. J. Environ. Manage. 249, 109390. https://doi.org/10.1016/j.jenvman.2019.109390.

[14] T. Santos, G. Cancian, D.N.R. Neodini, D.R.S. Mano, C. Capucho, F.S. Predes, R. Barbieri, C.A. Oliveira, A.A. Pigoso, H. Dolder, G.D.C. Severi-Aguiar, Toxicological

evaluation of ametryn effects in Wistar rats, Exp. Toxicol. Pathol. 67 (2015) 525–532. http://dx.doi.org/10.1016/j.etp.2015.08.001.

[15] G.L. Scheel, C.R.T. Tarley, Feasibility of supramolecular solvent-based microextraction for simultaneous preconcentration of herbicides from natural waters with posterior determination by HPLC-DAD, Microchem. J. 133 (2017) 650–657. http://dx.doi.org/10.1016/j.microc.2017.03.007.

[16] S. Sangami, B. Manu, Fenton's treatment of actual agriculture runoff water containing herbicides, Water Sci Technol. 75 (2017) 451-461. https://doi.org/10.2166/wst.2016.538**.**

[17] P.N. Kunene, P.N. Mahlambi, 2019. Development and application of SPE-LC-PDA method for the determination of triazines in water and liquid sludge samples. J. Environ. Manage. 249, 109415. https://doi.org/10.1016/j.jenvman.2019.109415.

[18] V. Salvatierra-stamp, R. Muñiz-Valencia, J.M. Jurado, S.G. Ceballos-Magaña, Hollow fiber liquid phase microextraction combined with liquid chromatography-tandem mass spectrometry for the analysis of emerging contaminants in water samples, Microchem. J. 140 (2018) 87–95. https://doi.org/10.1016/j.microc.2018.04.012.

[19] X. Wang, R. Jia, Y. Song, M. Wang, Q. Zhao, S. Sun, 2019. Determination of pesticides and their degradation products in water samples by solid-phase extraction coupled with liquid chromatography-mass spectrometry. Microchem. J. 149, 104013. https://doi.org/10.1016/j.microc.2019.104013.

[20] L.C. Friedrich, M.A. Mendes, V.O. Silva, C.L.P.S. Zanta, A. Machulek, Jr., F.H. Quina, Mechanistic implications of zinc (II) ions on the degradation of phenol by the fenton reaction, J. Braz. Chem. Soc. 23 (2012) 1372-1377. http://dx.doi.org/10.1590/S0103-50532012000700022.

[21] A. Machulek Jr., F.H. Quina, F. Gozzi, V.O. Silva, L.C. Friedrich, J.E.F. Moraes, Fundamental mechanistic studies of the photo-Fenton reaction for the degradation of organic pollutants, in: T. Puzyn, A. Mostrag-Szlichtyng (Eds.), Organic Pollutants Ten Years After the Stockholm Convention - Environmental and Analytical Update, IntechOpen., 2012, pp. 271-292. DOI: 10.5772/30995. Available from: https://www.intechopen.com/books/organic-pollutants-ten-years-after-the-stockholm-convention-environmental-and-analytical-update/fundamental-mechanistic-studies-of-the-photo-fenton-reaction-for-the-degradation-of-organic-pollutan.

[22] D.C. Castro, R.P. Cavalcante, J. Jorge, M.A.U. Martines, L.C.S. Oliveira, G.A. Casagrande, A. Machulek Jr., Synthesis and characterization of mesoporous Nb_2O_5 and its application for photocatalytic degradation of the herbicide methylviologen, J. Braz. Chem. Soc. 27 (2016) 303-313. http://dx.doi.org/10.5935/0103-5053.20150244.

[23] R.P. Cavalcante, R.F. Dantas, H. Wender, B. Bayarri, O. González, J. Giménez, S. Esplugas, A. Machulek, Jr., Photocatalytic treatment of metoprolol with B-doped TiO_2: Effect of water matrix, toxicological evaluation and identification of intermediates, Appl. Catal. B: Environ. 176-177 (2015) 173-182. https://doi.org/10.1016/j.apcatb.2015.04.007.

[24] R.P. Cavalcante, R.F. Dantas, B. Bayarri, O. González, J. Giménez, S. Esplugas, A. Machulek, Jr., Synthesis and characterization of B-doped TiO_2 and their performance for the degradation of metoprolol, Catal. Today. 252 (2015) 27–34. https://doi.org/10.1016/j.cattod.2014.09.030.

[25] V. Augugliaro, M. Bellardita, V. Loddo, G. Palmisano, L. Palmisano, S. Yurdakal, Overview on oxidation mechanisms of organic compounds by TiO_2 in heterogeneous photocatalysis, J. Photoch. Photobio. C. 13 (2012) 224–245. http://dx.doi.org/10.1016/j.jphotochemrev.2012.04.003.

[26] S. Horikoshi, N. Serpone, Can the photocatalyst TiO_2 be incorporated into a wastewater treatment method? Background and prospects, Catal. Today 340 (2018) 334-346. https://doi.org/10.1016/j.cattod.2018.10.020.

[27] M. Pelaez, N.T. Nolan, S.C. Pillai, M.K. Seery, P. Falaras, A.G. Kontos, P.S.M. Dunlop, J.W.J. Hamilton, J.A. Byrne, K. O'Shea, M.H. Entezari, D.D. Dionysiou, A review on the visible light active titanium dioxide photocatalysts for environmental applications, Appl. Catal. B. 125 (2012) 331–349, http://dx.doi.org/10.1016/j.apcatb.2012.05.036.

[28] A.O. Ibhadon, P. Fitzpatrick, Heterogeneous photocatalysis: Recent advances and applications, Catalysts. 3 (2013) 189-218. https://doi.org/10.3390/catal3010189.

[29] J. Kumar, A. Bansal, Photocatalysis by nanoparticles of titanium dioxide for drinking water purification: A conceptual and state-of-art review, Mater. Sci. Forum. 764 (2013) 130-150. https://doi.org/10.4028/www.scientific.net/MSF.764.130.

[30] X. Jiang, M. Manawan, T. Feng, R. Qian, T. Zhao, G. Zhou, F. Kong, Q. Wang, S. Dai, J.H. Pan, Anatase and rutile in evonik aeroxide P25: Heterojunctioned or individual nanoparticles?, Catal. Today 300 (2018) 12–17. http://dx.doi.org/10.1016/j.cattod.2017.06.010.

[31] K. Wetchakun, N. Wetchakun, S. Sakulsermsuk, An overview of solar/visible light-driven heterogeneous photocatalysis for water purification: TiO_2- and ZnO-based photocatalysts used in suspension photoreactors, J. Ind. Eng. Chem. 71 (2019) 19–49. https://doi.org/10.1016/j.jiec.2018.11.025.

[32] R. Palominos, J. Freer, M.A. Mondaca, H.D. Mansilla, Evidence for hole participation during the photocatalytic oxidation of the antibiotic flumequine, J. Photochem. Photobiol. A. Chem. 193 (2008) 139–145. https://doi.org/10.1016/j.jphotochem.2007.06.017.

[33] P. Ribao, J. Corredor, M.J. Rivero, I. Ortiz, Role of reactive oxygen species on the activity of noble metal-doped TiO_2 photocatalysts, J. Hazard. Mater. 372 (2019) 45-51. https://doi.org/10.1016/j.jhazmat.2018.05.026.

[34] R.P. Cavalcante, R.F. Dantas, B. Bayarri, O. Gonzalez, J. Giménez, S. Esplugas, A. Machulek Jr., Photocatalytic mechanism of metoprolol oxidation by photocatalysts TiO_2 and TiO_2 doped with 5% B: primary active species and intermediates, Appl. Catal. B. 194 (2016) 111–122. https://doi.org/10.1016/j.apcatb.2016.04.054.

[35] L. Ismail, A. Rifai, C. Ferronato, L. Fine, F. Jaber, J-M. Chovelon, Towards a better understanding of the reactive species involved in thephotocatalytic degradation of sulfaclozine, Appl. Catal. B. 185 (2016) 88–99. http://dx.doi.org/10.1016/j.apcatb.2015.12.008.

[36] T. Jedsukontorn, T. Ueno, N. Saito, M. Hunsom, Mechanistic aspect based on the role of reactive oxidizing species (ROS) in macroscopic level on the glycerol photooxidation over defected and defected-free TiO_2, J. Photochem. Photobiol. A Chem. 367 (2018) 270–281. https://doi.org/10.1016/j.jphotochem.2018.08.030.

[37] H-Y. Ma, L. Zhao, L-H. Guo, H. Zhang, F.-J. Chen, W-C. Yu, Roles of reactive oxygen species (ROS) in the photocatalytic degradation of pentachlorophenol and its main toxic intermediates by TiO_2/UV, J. Hazard. Mater. 369 (2019) 719-726. https://doi.org/10.1016/j.jhazmat.2019.02.080.

[38] Z. Xu, C. Jing, F. Li, X. Meng, Mechanisms of Photocatalytical Degradation of Monomethylarsonic and Dimethylarsinic Acids Using Nanocrystalline Titanium Dioxide, Environ. Sci. Technol. 42 (2008) 2349–2354. https://doi.org/10.1021/es0719677.

[39] M. Pelaez, P. Falaras, V. Likodimos, K. O'Shea, A.A. de la Cruz, P.S.M. Dunlop, J.A. Byrne, D.D. Dionysiou. Use of selected scavengers for the determination of NF-TiO_2 reactive oxygen species during the degradation of microcystin-LR under visible light irradiation. J. Mol. Catal. A: Chem. 425 (2016) 183–189. http://dx.doi.org/10.1016/j.molcata.2016.09.035.

[40] L. Cheng, C. Wei, Degradation of ametryn in aqueous solution by solar/S-doped titanium dioxide process, Adv. Mat. Res. 113-116 (2010) 1375-1378. https://doi.org/10.4028/www.scientific.net/AMR.113-116.1375.

[41] J. Colina-Márquez, F. Machuca-Martínez, G. Li Puma, Photocatalytic mineralization of commercial herbicides in a pilot-scale solar CPC reactor: photoreactor modeling and reaction kinetics constants independent of radiation field, Environ. Sci. Technol. 43 (2009) 8953-8960. https://doi.org/10.1021/es902004b.

[42] M. Dawson, G.B. Soares, C. Ribeiro, Preparation and photocatalytical performance of TiO_2:SiO_2 nanocomposites produced by the polymeric precursors method, J. Nanosci. Nanotechnol. 13 (2013) 5126-5133. https://doi.org/10.1166/jnn.2013.7603.

[43] G. Li, H. Zhang, C. Wei, Y. Huang, X. Dou, Y. Wang, J. Wang, Y. Song, Preparation of (5.0%)Er^{3+}:$Y_3Al_5O_{12}$/Pt-(TiO_2-Ta_2O_5) nanocatalysts and application in sonocatalytic decomposition of ametryn in aqueous solution, Ultrason. Sonochem. 34 (2017) 763–773. http://dx.doi.org/10.1016/j.ultsonch.2016.07.009.

[44] M.P. Ormad, N. Miguel, M. Lanao, R. Mosteo, J.L. Ovelleiro, Effect of application of ozone and ozone combined with hydrogen peroxide and titanium dioxide in the removal of pesticides from water, Ozone. Sci. Eng. 32 (2010) 25–32. http://dx.doi.org/10.1080/01919510903482764.

[45] G.B. Soares, B. Bravin, C.M.P. Vaz, C. Ribeiro, Facile synthesis of N-doped TiO_2 nanoparticles by a modified polymeric precursor method and its photocatalytic properties. Appl. Catal. B. 106 (2011) 287– 294. https://doi.org/10.1016/j.apcatb.2011.05.018.

[46] N. De la Cruz, V. Romero, R.F. Dantas, P. Marco, B. Bayarri, J. Giménez, S. Esplugas, o-Nitrobenzaldehyde actinometry in the presence of suspended TiO_2 for photocatalytic reactors, Catal. Today. 209 (2013) 209–214. https://doi.org/10.1016/j.cattod.2012.08.035.

[47] A.E. Greenberg, L.S. Clesceri, A.D. Eaton, Standard Methods for Examination of Water & Wastewater. 21st ed. American Public Health Association (APHA), American Water Works Association (AWWA) & Water Environment Federation (WEF), Washington, DC, 2005.

[48] L. Wojnárovits, E. Takács, Rate coefficients of hydroxyl radical reactions with pesticide molecules and related compounds: A review, Radiat. Phys. Chem. 96 (2014) 120-134. https://doi.org/10.1016/j.radphyschem.2013.09.003.

[49] D.M. de Oliveira, R.P. Cavalcante, L.M. da Silva, C. Sans, S. Esplugas, S.C. de Oliveira, A. Machulek Jr., Identification of intermediates, acute toxicity removal, and kinetics investigation to the ametryn treatment by direct photolysis (UV_{254}), UV_{254}/H_2O_2, Fenton, and photo-Fenton processes, Environ. Sci. Pollut. Res. Int. 26 (2019) 4348–4366. https://doi.org/10.1007/s11356-018-1342-6.

[50] V. Romero, N. De la Cruz, R.F. Dantas, P. Marco, J. Giménez, S. Esplugas, Photocatalytic treatment of metoprolol and propranolol, Catal. Today. 161 (2011) 115–120. https://doi.org/10.1016/j.cattod.2010.09.026.

[51] D. Juretic, H. Kusic, N. Koprivanac, A. L. Bozic, Photooxidation of benzene-structured compounds: Influence of substituent type on degradation kinetic and sum water parameters, Water. Res. 46 (2012) 3074-3084. https://doi.org/10.1016/j.watres.2012.03.014.

[52] S. Salaeh, D.J. Perisic, M. Biosic, H. Kusic, S. Babic, U.L. Stangar, D.D. Dionysiou, A.L. Bozic, Diclofenac removal by simulated solar assisted photocatalysis using TiO_2-based zeolite catalyst; mechanisms, pathways and environmental aspects, Chem. Eng. J. 304 (2016) 289–302. https://doi.org/10.1016/j.cej.2016.06.083.

[53] A.P.S. Batista, A.C.S.C. Teixeira, W.J. Cooper, B.A. Cottrell, Correlating the chemical and spectroscopic characteristics of natural organic matter with the photodegradation of sulfamerazine, Water. Res. 93 (2016) 20-29. http://dx.doi.org/10.1016/j.watres.2015.11.036.

[54] L. Rizzo, Bioassays as a tool for evaluating advanced oxidation processes in water and wastewater treatment, Water Res. 45 (2011) 4311-4340. https://doi.org/10.1016/j.watres.2011.05.035.

[55] F. Al-Momani, E. Touraud, J.R. Degorce-Dumas, J. Roussy, O. Thomas, Biodegradability enhancement of textile dyes and textile wastewater by VUV photolysis, J. Photochem. Photobiol. A, Chem. 153 (2002) 191–197. https://doi.org/10.1016/S1010-6030(02)00298-8.

[56] E.M. Rodríguez, G. Márquez, M. Tena, P.M. Álvarez, F.J. Beltrán, Determination of main species involved in the first steps of TiO_2 photocatalytic degradation of organics with the use

of scavengers: The case of ofloxacin. Appl. Catal. B. 178 (2015) 44–53. http://dx.doi.org/10.1016/j.apcatb.2014.11.002.

[57] W. Li, D. Li, J. Wang, Y. Shao, J. You, F. Teng, Exploration of the active species in the photocatalytic degradation ofmethyl orange under UV light irradiation, J. Mol. Catal. A: Chem. 380 (2013) 10–17. http://dx.doi.org/10.1016/j.molcata.2013.09.001.

[58] L. Chen, C. Zhao, D.D. Dionysiou, K.E. O'Shea, TiO_2 photocatalytic degradation and detoxification of cylindrospermopsin, J. Photochem. Photobiol. A, Chem. 307–308 (2015) 115–122. https://doi.org/10.1016/j.jphotochem.2015.03.013.

[59] T. Fotiou, T.M. Triantis, T. Kaloudis, K.E. O'Shea, D.D. Dionysiou, A. Hiskia, Assessment of the roles of reactive oxygen species in the UV and visible light photocatalytic degradation of cyanotoxins and water taste and odor compounds using $CeTiO_2$, Water. Res. 90 (2016) 52-61. http://dx.doi.org/10.1016/j.watres.2015.12.006.

[60] A. Tiwari, A. Shukla, Lalliansanga, D. Tiwari, S.M. Lee, Nanocomposite thin films Ag^0(NP)/TiO_2 in the efficient removal of micropollutants from aqueous solutions: A case study of tetracycline and sulfamethoxazole removal, J. Environ. Manage. 220 (2018) 96–108. https://doi.org/10.1016/j.jenvman.2018.05.019.

[61] P. Raja, A. Bozzi, H. Mansilla, J. Kiwi, Evidence for superoxide-radical anion, singlet oxygen and OH-radical intervention during the degradation of the lignin model compound (3-methoxy-4-hydroxyphenylmethylcarbinol), J. Photochem. Photobiol. A: Chem. 169 (2005) 271–278. https://doi.org/10.1016/j.jphotochem.2004.07.009.

[62] S. Zheng, Y. Cai, K.E. O'Shea, TiO_2 photocatalytic degradation of phenylarsonic acid. J. Photochem. Photobiol. A: Chem. 210 (2010) 61–68. https://doi.org/10.1016/j.jphotochem.2009.12.004.

[63] G.V. Buxton, C.L. Greenstock, W.P. Helman, A.B. Ross, Critical review of rate constants for reactions of hydrated electrons, hydrogen atoms and hydroxyl radicals (˙OH/˙O−) in aqueous solution, J. Phys. Chem. Ref. Data. 17 (1988) 513. https://doi.org/10.1063/1.555805.

[64] M. Anbar, P. Neta, a compilation of specific bimolecular rate constants for the reactions of hydrated electrons, hydrogen atoms and hydroxyl radicals with inorganic and organic compounds in aqueous solution, Int. J. Appl. Radiat. Isotopes. 18 (1967) 493–523. https://doi.org/10.1016/0020-708X(67)90115-9.

[65] A. Samad, S. Ahsan, I. Tateishi, M. Furukawa, H. Katsumata, T. Suzuki, S. Kaneco, Indirect photocatalytic reduction of arsenate to arsenite in aqueous solution with TiO_2 in the presence of hole scavengers, Chin. J. Chem. Eng. 26 (2018) 529–533. https://doi.org/10.1016/j.cjche.2017.05.019.

[66] F.J. Benitez, J.L. Acero, F.J. Real, S. Roman, Oxidation of MCPA and 2,4-D by UV radiation, ozone, and the combinations UV/H_2O_2 and O_3/H_2O_2. J. Environ. Sci. Health., Part B, 39 (2004) 393–409. https://doi.org/10.1081/PFC-120035925.

[67] R.F. Dantas, S. Contreras, C. Sans, S. Esplugas, Sulfamethoxazole abatement by means of ozonation, J. Hazard. Mater. 150 (2008) 790–794. https://doi.org/10.1016/j.jhazmat.2007.05.034.

[68] H. Zeghioud, M. Kamagate, L.S. Coulibaly, S. Rtimi, A.A. Assadi, Photocatalytic degradation of binary and ternary mixtures of antibiotics: reactive species investigation in pilot scale, Chem. Eng. Res. Des. 144 (2019) 300–309. https://doi.org/10.1016/j.cherd.2019.02.015.

[69] L.M. da Silva, R.P. Cavalcante, R.F. Cunha, F. Gozzi, R.F. Dantas, S.C. de Oliveira, A. Machulek Jr, Tolfenamic acid degradation by direct photolysis and the UV-ABC/H_2O_2 process: factorial design, kinetics, identification of intermediates, and toxicity evaluation, Sci. Total. Environ. 573 (2016) 518–531. https://doi.org/10.1016/j.scitotenv.2016.08.139.

[70] B.A. Wols, C.H.M. Hofman-Caris, Review of photochemical reaction constants of organic micropollutants required for UV advanced oxidation processes in water, Water. Res. 46 (2012) 2815–2827. https://doi.org/10.1016/j.watres.2012.03.036.

[71] C. Wu, K.G. Linden, Phototransformation of selected organophosphorus pesticides: Roles of hydroxyl and carbonate radicals, Water. Res. 44 (2010) 3585-3594. https://doi.org/10.1016/j.watres.2010.04.011.

[72] T. Chen, Z. Liu, J. Yao, H. Hao, F. Chen, Fenton-like degradation comparison of s-triazine herbicides in aqueous medium, Clean-*Soil Air Water*. 44 (2016) 1315–1322. https://doi.org/10.1002/clen.201500304.

[73] C. Jiang, Y. Yang, L. Zhang, D. Lu, L. Lu, X. Yang, T. Cai, 2020. Degradation of atrazine, simazine and ametryn in an arable soil using thermal-activated persulfate oxidation process: Optimization, kinetics, and degradation pathway, J. Hazard. Mater. 400, 123201. https://doi.org/10.1016/j.jhazmat.2020.123201.

[74] W. Yang, Y. Tang, L. Liu, X. Peng, Y. Zhong, Y. Chen, Y. Huang, 2020. Chemical behaviors and toxic effects of ametryn during the UV/chlorine process. Chemosphere. 240, 124941. https://doi.org/10.1016/j.chemosphere.2019.124941.

[75] F. Gozzi, I. Sirés, A. Thiam, S.C. de Oliveira, A. Machulek Jr, E. Brillas, Treatment of single and mixed pesticide formulations by solar photoelectro-Fenton using a flow plant, Chem. Eng. J. 310 (2017) 503–513. https://doi.org/10.1016/j.cej.2016.02.026.

[76] A. Lopez, G. Mascolo, G. Tiravanti, R. Passino, Degradation of herbicides (ametryn and isoproturon) during water disinfection by means of two oxidants (hypochlorite and chlorine dioxide), Water. Sci. Technol. 35 (1997) 129–130, 132-136. https://doi.org/10.1016/S0273-1223(97)00018-8.

[77] G. Mascolo, A. Lopez, R. Passino, G. Ricco, G. Tiravanti, Degradation of sulphur containing s-triazines during water chlorination, Water. Res. 28 (1994) 2499–2506. https://doi.org/10.1016/0043-1354(94)90068-X.

[78] C-G. Liu, J-N. Shu, B. Yang, P. Zhang. Products and kinetics of the heterogeneous reaction of particulate ametryn with NO_3 radicals, Environ. Sci. Process. Impacts. 16 (2014) 2686-2691. https://doi.org/10.1039/c4em00352g.

[79] S.S. AlSaleem, W.M. Zahid, I.M. Alnashef, H. Haider, Destruction of environmentally hazardous halogenated hydrocarbons in stable ionic liquids with superoxide ion radical, Sep. Purif. Technol. 215 (2019) 134–142. https://doi.org/10.1016/j.seppur.2018.12.070.

[80] D. Vialaton, C. Richard, Phototransformation of aromatic pollutants in solar light: Photolysis versus photosensitized reactions under natural water conditions, Aquat. Sci. 64 (2002) 207–215. https://doi.org/10.1007/s00027-002-8068-7.

[81] C.A. Aggelopoulos, D. Tataraki, G. Rassias, Degradation of atrazine in soil by dielectric barrier discharge plasma – Potential singlet oxygen mediation, Chem. Eng. J. 347 (2018) 682–694. https://doi.org/10.1016/j.cej.2018.04.111.

[82] A.G. Griesbeck, B. Goldfuss, M. Leven, A. de Kiff, Comparison of the singlet oxygen ene reactions of cyclic versus acyclic β,γ-unsaturated ketones: an experimental and computational study, Tetrahedron. Lett. 54 (2013) 2938–2941. https://doi.org/10.1016/j.tetlet.2013.03.099.

[83] M. Stratakis, M. Orfanopoulos, Regioselectivity in the ene reaction of singlet oxygen with alkenes, Tetrahedron. 56 (2000) 1595–1615. https://doi.org/10.1016/s0040-4020(99)00950-3.

[84] P. Sun, H. Liu, M. Feng, L. Guo, Z. Zhai, Y. Fang, X. Zhang, V.K. Sharma, Nitrogen-sulfur co-doped industrial graphene as an efficient peroxymonosulfate activator: Singlet oxygen-dominated catalytic degradation of organic contaminants, Appl. Catal. B. 251 (2019) 335–345. https://doi.org/10.1016/j.apcatb.2019.03.085.

[85] J. Trawiński, R. Skibiński, Rapid degradation of clozapine by heterogeneous photocatalysis. Comparison with direct photolysis, kinetics, identification of transformation products and scavenger study, Sci. Total. Environ. 665 (2019) 557–567. https://doi.org/10.1016/j.scitotenv.2019.02.124.

Supplementary Material

Evaluation of the main active species involved in the TiO_2 photocatalytic degradation of ametryn herbicide and its by-products

Rodrigo Pereira Cavalcante[1,3], Dirce Martins de Oliveira[2], Lucas de Melo da Silva[1], Jaime Giménez[3], Santiago Esplugas[3], Silvio César de Oliveira[1], Renato Falcão Dantas[3], Carme Sans[3]*, Amilcar Machulek Junior[1,2]**

(*1) Institute of Chemistry, Federal University of Mato Grosso do Sul, Av. Senador Filinto Muller, 1555, CP 549, CEP 79074-460- Campo Grande, MS, Brazil.*

(2) Faculty of Engineering, Architecture and Urbanism and Geography, Federal University of Mato Grosso do Sul, Cidade Universitária, CP 549, CEP 79070-900 Campo Grande, MS, Brazil.

(3) Department of Chemical Engineering and Analytical Chemistry, Faculty of Chemistry, Universitat de Barcelona, C/Martí i Franqués 1, 08028 Barcelona, Spain

**Corresponding author: E-mail address: machulekjr@gmail.com (A. Machulek Jr.)

*Corresponding author: E-mail address: carmesans@ub.edu (Carme Sans)

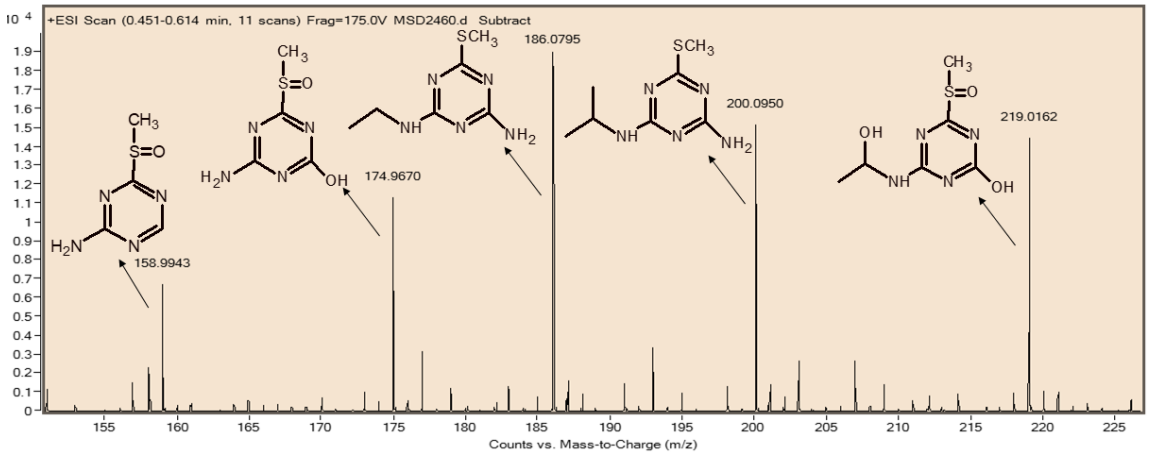

Fig. S1. LC/MS spectrum model of by-products of ametryn degradation formed during the photocatalytic process using TiO_2 P25.

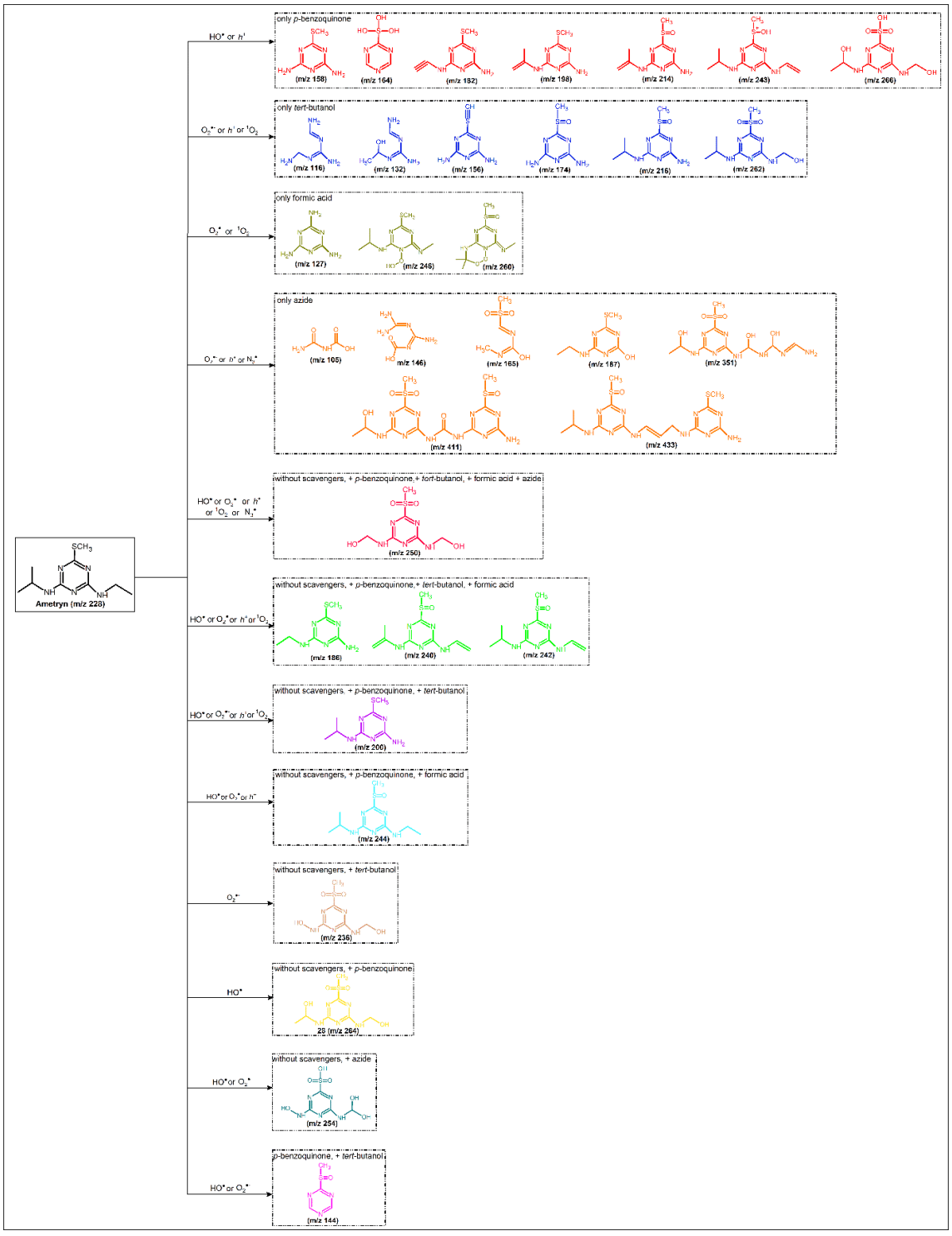

Fig. S2. Scheme showing the possible ROS involved in the generation of by-products resulting from the photocatalytic degradation of ametryn observed by LC/MS using comercial TiO_2 in the presence of specific scavengers.